1974

A five-particle, shell-model calculation using a spin-dependent potential as applied to 101Tc and the nuclear decays of 101Mo, 101Tc, 142Xe, and 142Cs

James Foley Wright
Iowa State University

WRIGHT, James Foley, 1943-

A FIVE-PARTICLE, SHELL-MODEL CALCULATION USING A SPIN-DEPENDENT POTENTIAL AS APPLIED TO ^{101}Tc AND THE NUCLEAR DECAYS OF ^{101}Mo, ^{101}Tc, ^{142}Xe, AND ^{142}Cs.

Iowa State University, Ph.D., 1974
Chemistry, nuclear

A five-particle, shell-model calculation using a spin-dependent potential as applied to ^{101}Tc and the nuclear decays of ^{101}Mo, ^{101}Tc, ^{142}Xe, and ^{142}Cs

by

James Foley Wright

A Dissertation Submitted to the

Graduate Faculty in Partial Fulfillment of

The Requirements for the Degree of

DOCTOR OF PHILOSOPHY

Department: Chemistry
Major: Physical Chemistry

Approved:

Signature was redacted for privacy.

In Charge of Major Work

Signature was redacted for privacy.

For the Major Department

Signature was redacted for privacy.

For the Graduate College

Iowa State University
Ames, Iowa

1974

TABLE OF CONTENTS

LIST OF TABLES

LIST OF FIGURES

I. SHELL-MODEL CALCULATION

A. Introduction

A main goal of experimental nuclear structure studies is to verify or contradict the many hypotheses underlying various theories of the nucleus. With the great volumes of experimental data that are being gathered and published, it has become impossible for the experimentalists to rely solely on the theorists to compare their experiments with the theory. In fact, it is becoming increasingly clear that complete theoretical work should accompany experimental efforts. This allows the development of a more complete investigation and encourages the determination of the most pertinent experiments.

The objective of this part of the investigation is to produce a single model that will adequately compare with the experimental energy levels of the 43-proton nucleus ^{101}Tc. Shell-model calculations by Auerbach and Talmi (1) give a ground-state wave function of 88% $(g_{9/2})^3(p_{1/2})^2$ and 12% $(g_{9/2})^5$ for ^{99}Tc. Similar calculations by Vervier (2) predict the ground-state wave function to be 76% $(g_{9/2})^3(p_{1/2})^2$ and 24% $(g_{9/2})^5$. The single-particle shell model does not produce the large number of low-lying states that are seen experimentally. The many-particle shell model produces a large number of low-lying states. If this theory is adequate, the calculation should provide insight into the

wave function construction and spins and parities of the levels.

1. Single-particle model

The single-particle shell model (SPM) is a phenomenological model which has had a certain amount of success in predicting such nuclear properties as ground-state spins and parities and nuclear magnetic moments. It was formulated by Mayer (3) under the assumption that the nucleons move independently in an average, central potential and that the properties of the lowest states in odd-A nuclei are determined only by the last unpaired nucleon. The other nucleons are paired to make no contribution to these properties and the average, central potential is equivalent to assuming a spherical nucleus. This is substantiated in that nuclei with an even number of nucleons have a ground state spin of J=0.

Experimental evidence gives an indication of "magic numbers", where extra stability is observed. This stability is manifested by the discontinuities in the nuclear binding energies for nucleon numbers 2, 8, 20, 28, 50, 82 and 126. These discontinuities indicate a large energy separation between the nuclear orbitals that belong to the different shells. This is analogous to the atomic case with the noble gases. When other orbitals are filled, smaller increases in stability are sometimes observed. These subshell effects

occur for nucleon numbers 6, 16, 38, and 58.

If a three-dimensional harmonic oscillator is taken as the average central potential, shell closure (magic numbers) is obtained at 2, 8, 20, 40, 70, 112, and 168 nucleons. A square well potential gives magic numbers at 2, 18, 20, 34, 40, 58, 68, 70, 92, 106, 112, 138, and 156 nucleons. These potentials compare poorly with experiment on the magic numbers. However, when a spin-orbit term is added to a harmonic oscillator potential, shell closure occurs at 2, 8, 20, 28, 50, 82, 126, and 184, in substantial agreement with experiment. The actual average nuclear potential is probably an interpolation between the square well and harmonic oscillator, with a spin-orbit contribution.

Near regions of "magic numbers", the nucleus is thought to be spherical. Exactly how spherical, or how close to these magic numbers the nucleus remains spherical, are basic questions for the nuclear spectroscopists. The ^{101}Tc nucleus, with 43 protons and 58 neutrons, is used in this research to test the shell model.

2. Many-particle shell model

The many-particle shell model is an extension of the SPM. Nucleons are distributed among single-particle states in such a manner that the Pauli Principle is not violated. The inner, or core, particles are all paired. It is assumed that the only particles that make a significant contribution

to the low-energy spectra are valence, or extra-core, nucleons. The interaction among these valence particle particles is commonly treated in first-order pertubation theory. Without this residual interaction, all states are degenerate at the single-particle energies. When the potential is turned on, the degeneracy of the non-interacting states is broken and they are split by an amount given by equation (1).

$$E = \langle J \mid V(\text{residual}) \mid J \rangle \qquad (1)$$

This residual interaction is actually the difference between the real nuclear Hamiltonian and the shell-model Hamiltonian as shown in equation (2).

$$H(\text{real}) = H(\text{SM}) + V(\text{residual})$$
$$V(\text{residual}) = H(\text{real}) - H(\text{SM}) \qquad (2)$$

A prime goal in nuclear chemistry and physics is to determine the exact form of the residual interaction, V(residual), and therefore determine the nuclear potential.

The eigenvalues of the single-particle states are treated as a separate problem. They can be calculated from Hartree-Fock theory or treated as is done in the present work.

B. Wave Function Construction

The wave function that is used must be an eigenfunction of the shell-model Hamiltonian. For this Hamiltonian we choose the harmonic-oscillator central potential with a spin-orbit $(\vec{\ell}\cdot\vec{s})$ term.

$$H(SM) = \sum_{i=1}^{N} h_i \tag{3}$$

$$h_i = \frac{p_i^2}{2m} + (1/2)\, m\omega_i^2 r_i^2 + a\vec{\ell}_i\cdot\vec{s}_i$$

Thus the single-particle basis states are of the form

$$|\Psi\rangle = \Phi(r)\ |jm\rangle$$

$$= \Phi(r) \sum_{m_\ell m_s} C(\ell s m_\ell m_s | jm)\ Y_{\ell m_\ell}\ \chi_{m_s}. \tag{4}$$

The spherical harmonic of degree k and projection n is symbolized by Y_{kn}. χ_n is a spinor of projection n that represents the spin dependence of the nuclear wave function and $\Phi(r)$ is the radial portion of the wave function (4). The $C(jjm_1 m_2 | JM)$ is a Clebsch-Gordan coefficient (5) coupling angular momentum j, with projection m_1, to angular momentum j, with projection m_2, to angular momentum J with projection M. The wave function that is convenient to use is constructed in the following manner. We assume that the spin, s_i, and the orbital angular momentum, ℓ_i, of particle i are coupled to give the particle angular momentum j_i.

$$s_i \otimes \ell_i = j_i \tag{5}$$

In constructing the many-particle wave function, the angular momenta of each of the particles i and k are coupled to give a total angular momentum J_k. The next particle, with angular momentum j_ℓ, is coupled to J_k to give J_ℓ. This procedure is repeated until the nth particle is coupled to J_{n-1} to give the total angular momentum J. This is the n-particle j-j coupled wave function. The shell-model Hamiltonian of equation (3) is diagonal in this representation.

The construction of n-particle wave functions can be illustrated by building on a simple, antisymmetric two-particle wave function. A two-particle wave function can be constructed in the following manner.

$$|j^2 J\rangle = \sum_{m_1 m_2} C(jjm_1m_2|JM)\ |jm_1\rangle_{\underline{1}}\ |jm_2\rangle_{\underline{2}} \tag{6}$$

The ket $|j_i m_i\rangle_{\underline{n}}$ represents a one-particle wave function with angular momentum j_i and projection of m_i of particle n (particle number is indicated by underlined subscripts). The antisymmetric two-particle wave function, written in terms of our un-antisymmetrized wave function $|j^2 J\rangle$, is

$$\frac{1}{2}\,\underline{A}|j^2 J> = \frac{[1 + (-1)^J]}{2}\,|j^2 J>$$

$$= |j^2 J> \qquad \text{if } J \quad \text{even.} \tag{7}$$

The antisymmetrizing operator is denoted by the symbol $\underline{A}$. For two particles

$$\underline{A}f(1)g(2) = f(1)g(2) - f(2)g(1). \tag{8}$$

The Pauli Principle requires the eigenfunctions for all nucleons in the nucleus to be antisymmetric with respect to exchange of any two of the nucleons.

Equation (9) is a three-particle wave function constructed by coupling the third particle to the already existent, antisymmetric two-particle wave function of equation (7). The coefficients that couple this last particle to the "parent" two-particle wave function, in such a manner to give a totally antisymmetric, normalized wave function, are called one-body coefficients of fractional parentage (CFP).

$$\underline{A}|j^3 \alpha J> = \sum_{\alpha_1 J_1} (j^2(\alpha_1 J_1) j; J|\}j^3\, J)\ [\ \underline{A}|j^2 \alpha_1 J_1> \otimes$$

$$|j>_{\underline{3}}]^J_M \tag{9}$$

Equation (9) indicates that a three-particle wave function of spin J and additional quantum numbers α is constructed from three single-particle wave functions of angular momentum j. The CFP is symbolized by $(j^2(\alpha_1 J_1) j; J|\}j^3 \alpha J)$. It must be noted that the antisymmetrizing operator, $\underline{A}$,

operates only on kets which it immediately precedes. In the same manner, equation (10) shows an n-particle wave function can be formed from an (n-1)-particle wave function by the proper one-body CFP.

$$\underline{A}|j^n\alpha J> = \sum_{\alpha_1 J_1} (j^{n-1}(\alpha_1 J_1)j;J|\}j^n\alpha J)\ [\underline{A}|j^{n-1}\alpha_1 J_1> \otimes |j>_{\underline{n}}\ ]^J_M \tag{10}$$

$$= \sum_{\alpha_1 J_1} (j^{n-1}(\alpha_1 J_1)j;J|\}j^n\alpha J)\ |j^{n-1}\alpha_1 J_1, j_{\underline{n}}; j^n\alpha JM> \tag{11}$$

The one-body CFP separates one particle from an n-particle wave function. The expansion of the wave function of equation (10) is useful in carrying out calculations involving one-body operators. An example of a one-body matrix element is given by equation (12).

$$<j^n\alpha J|\sum_{i=1}^{n} O_{\underline{i}}|j^n\alpha' J'> = n \sum_{\alpha_1 J_1} (j^{n-1}(\alpha_1 J_1)j;J|\}j^n\alpha J)\ \times$$

$$(j^{n-1}(\alpha_1 J_1)j;J'|\}j^n\alpha' J')\ <j_{\underline{n}}|O_{\underline{n}}|j_{\underline{n}}> \tag{12}$$

For calculations involving interactions between two particles, one needs to "separate" two particles from the n-particle wave function. This can be done by constructing two-body CFPs. The (n-1)-particle wave function on the right-hand side of equation (10) can be written in terms of its one-body CFP's as follows:

$$\underline{A}|j^{n-1}\alpha_1 J_1> = \sum_{\alpha_2 J_2} (j^{n-2}(\alpha_2 J_2)j;J_1|\}j^{n-1}\alpha_1 J_1) \times$$

$$|j^{n-2}\alpha_2 J_2, j_{\underline{n-1}}; j^{n-1}\alpha_1 J_1> . \qquad (13)$$

Substituting in equation (10), we obtain:

$$\underline{A}|j^n \alpha J> = \sum_{\alpha_1 J_1} \sum_{\alpha_2 J_2} (j^{n-2}(\alpha_2 J_2)j;J_1|\}j^{n-1}\alpha_1 J_1) \times$$

$$(j^{n-1}(\alpha_1 J_1)j;J|\}j^n \alpha J) \times$$

$$|j^{n-2}\alpha_2 J_2, j_{\underline{n-1}}(j^{n-1}\alpha_1 J_1), j_{\underline{n}}; j^n \alpha J> . \qquad (14)$$

The present coupling scheme represented in the last line is $[[\ J_2 \boxtimes j_{\underline{n-1}}]^{J_1} \boxtimes j_{\underline{n}}]^J$. The coupling $[\ J_2 \boxtimes [j_{\underline{n-1}} \boxtimes j_{\underline{n}}]^{J_0}]^J$ can be obtained using equation (15) to perform the transformation.

$$|j^{n-2}\alpha_2 J_2, j_{\underline{n-1}}(j^{n-1}\alpha_1 J_1), j_{\underline{n}}; j^n \alpha J> = \sum_{J_0} \times$$

$$< J_2, j_{\underline{n-1}}(J_1), j_{\underline{n}}; J \mid J_2, j_{\underline{n-1}} j_{\underline{n}}(J_0); J > \times$$

$$|j^{n-2}(\alpha_2 J_2), j^2(J_0); \alpha J> \qquad (15)$$

The 6-j symbol is defined by the transformation (6)

$$<J_2, j_{\underline{n-1}}(J_1), j_{\underline{n}}; J|J_2, j_{\underline{n-1}} j_{\underline{n}}(J_0); J> = (-1)^{2j+J_2+J} \times$$

$$[J_1][J_0] \begin{Bmatrix} J_2 & j & J_1 \\ j & J & J_0 \end{Bmatrix} , \qquad (16)$$

where $[j] = \sqrt{2j+1}$. By using equations (15) and (16), we

can rewrite equation (14) in the following manner:

$$\underline{A}|j^n\alpha J> = \sum_{\alpha_2 J_2 J_0} (j^{n-2}(\alpha_2 J_2), j^2(J_0); J|\}j^n\alpha J) \times$$

$$[\underline{A}|j^{n-2}\alpha_2 J_2> \otimes \underline{A}|j^2 J_0>]^J. \qquad (17)$$

Now $(j^{n-2}(\alpha_2 J_2), j^2(J_0); J|\}j^n\alpha J)$ is the two-body CFP connecting our (n-2)-particle wave function of spin J_2 and additional quantum numbers α_2, to the n-particle wave function of spin J and additional quantum numbers α.

The wave functions are now available for calculations involving 2-body interactions. The form of the matrix element of a two-body operator is given by equation (18).

$$<j^n\alpha J| \sum_{i<j} O_{\underline{ij}} |j^n\alpha' J'> = \frac{n(n-1)}{2} \sum_{J_0} \sum_{\alpha_2 J_2 J_0'} \sum \times$$

$$(j^{n-2}(\alpha_2 J_2) j^2(J_0); J|\}j^n\alpha J) \times$$

$$(j^{n-2}(\alpha_2 J_2) j^2(J_0); J'|\}j^n\alpha' J') \times$$

$$<j^2 J_0|O_{\underline{n,n-1}}|j^2 J_0'> \qquad (18)$$

C. Two-Body Interaction

The nucleon-nucleon interaction is by definition a two-body force and its short range is verified by the size of the nucleus. The fact that the scattering cross sections for pp and nn scattering are nearly the same implies approximate charge independence for the interaction. A spin

dependence for the interaction is inferred by, for instance, np scattering cross section differences between ortho- and para-hydrogen. In the zero-range limit for the two-body interaction the force is proportional to a Dirac delta function. The delta interaction is composed of a radial part and an angular part as shown in equation (19).

$$G\delta(\vec{r}_1-\vec{r}_2) = \frac{G\delta(r_1-r_2)}{r_1 r_2} \sum_\lambda Y_\lambda(\hat{r}_1)\cdot Y(\hat{r}_2) \qquad (19)$$

where $Y_\lambda \cdot Y_\lambda = \sum_\mu Y_{\lambda\mu}\, Y^*_{\lambda\mu}$

The Y (r) is a spherical harmonic representing the angular coordinates of particle i (7). The G is proportional to the strength of the interaction. The angular portion of the two-body delta function matrix element can be derived using standard Racah techniques and is given below.

$$\sum_\lambda \langle j_1 j_2 J_0 | Y_\lambda \cdot Y_\lambda | j_3 j_4 J_0\rangle = \frac{1}{4\pi}(-1)^{j_2+j_4+J_0} \sum_\lambda [\lambda]^2 \times$$

$$[j_1][j_2][j_3][j_4] \begin{Bmatrix} j_1 & j_2 & J_0 \\ j_4 & j_3 & \lambda \end{Bmatrix} \begin{pmatrix} j_1 & j_3 & \lambda \\ \frac{1}{2} & -\frac{1}{2} & 0 \end{pmatrix}\begin{pmatrix} j_2 & j_4 & \lambda \\ \frac{1}{2} & -\frac{1}{2} & 0 \end{pmatrix} \times$$

$$Z(\ell_1 \ell_3 \lambda)\; Z(\ell_2 \ell_4 \lambda)$$

$$\text{where } (j_1 j_2 m_1 m_2 | jm) = (-1)^{j_2-j_1-m}[j]\begin{pmatrix} j_1 & j_2 & J \\ m_1 & m_2 & -m \end{pmatrix} \qquad (20)$$

Equation (20) is the angular portion of a delta function matrix element between two particles of total angular momenta j_1 and j_2 coupled to J_0, interacting with two

particles of total angular momenta j_3 and j_4 coupled to J_0. The symbol, Z(a,b,c), vanishes unless a, b and c form a triangle. Z also vanishes if a+b+c=odd, otherwise Z(a,b,c)=1. The delta interaction gives a "pairing spectrum" that is shown in Figure 1. A pairing spectrum is characterized by a large energy gap between the paired state (J=0) and the unpaired states (J≠0). No change is made in the ordering of the levels or shape of the spectra by varying the strength of the interaction.

When a spin-dependent term is added to a delta interaction, we get a more flexible potential. The operators $\vec{\sigma}_1 \cdot \vec{\sigma}_2$ and I (the identity operator) are the most general scalar spin-dependent terms which can be constructed from the variables describing a two-particle system. These operators are also subject to invariance under reflection, time reversal and particle exchange. The two-body, spin-dependent potential is given by equation (21).

$$V(1,2) = -G\delta(\vec{r}_1-\vec{r}_2)[1 - \alpha + \alpha\vec{\sigma}_1\cdot\vec{\sigma}_2] \quad 0 \leq \alpha \leq 1 \qquad (21)$$

The two-body matrix element of equation (21) is as follows:

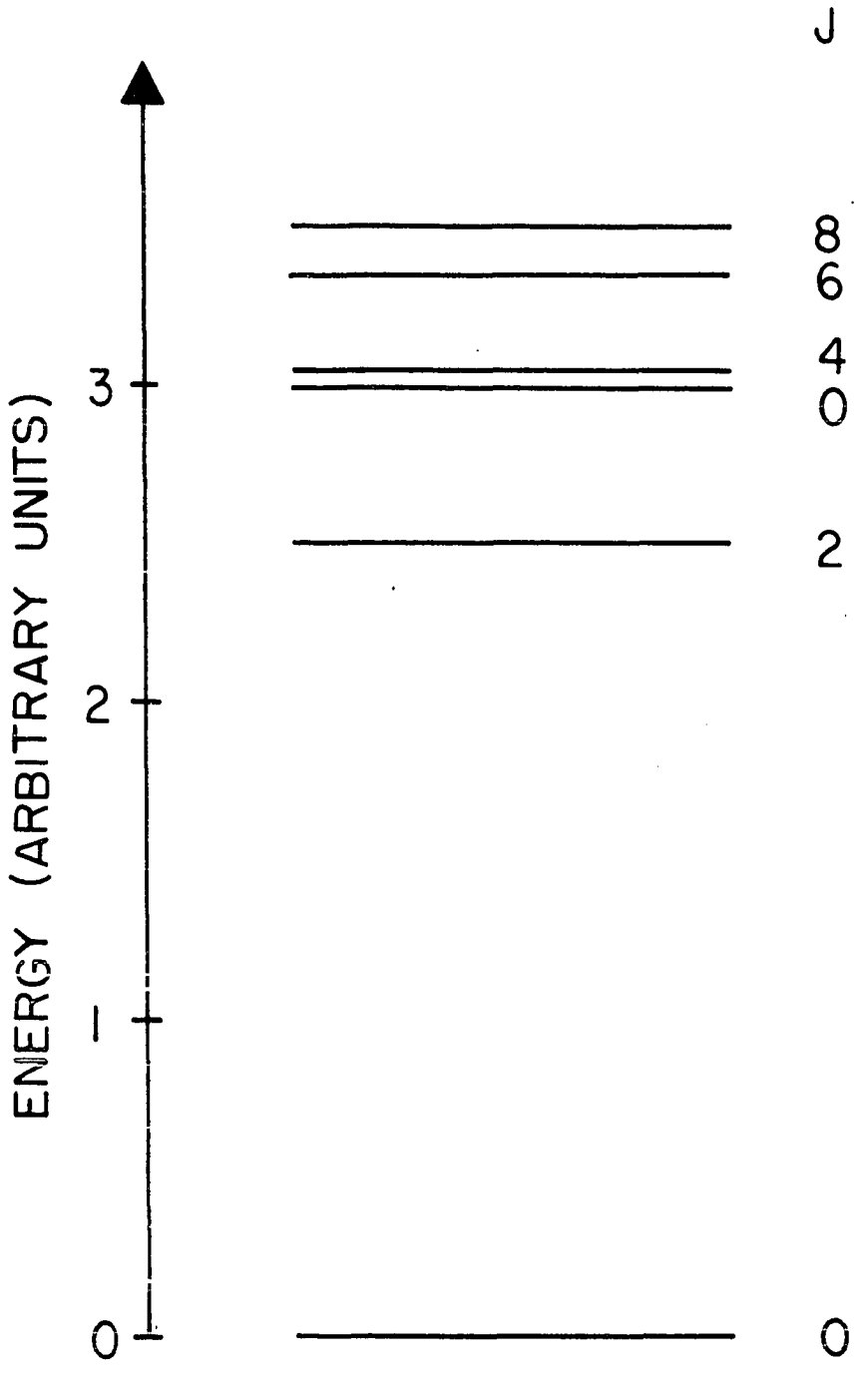

Figure 1. Eigenvalues of a delta-force interaction for the $(g_{9/2})^2(p_{1/2})^0$ and $(g_{9/2})^0(p_{1/2})^2$ configurations

$$\langle j_1 j_2 J|V(1,2)|j_3 j_4 J\rangle = \langle j_1 j_2 J|-G\delta(\vec{r}_1-\vec{r}_2)|j_3 j_4 J\rangle +$$

$$2[j_1][j_2][j_3][j_4](-1)^{\ell_1+\ell_3+j_2+j_4}\begin{Bmatrix}\ell_1 & \ell_2 & J\\ j_2 & j_1 & \frac{1}{2}\end{Bmatrix} x$$

$$\begin{Bmatrix}\ell_3 & \ell_4 & J\\ j_4 & j_3 & \frac{1}{2}\end{Bmatrix}\langle \ell_1 \ell_2 J|-G\alpha\delta(\vec{r}_1-\vec{r}_2)|\ell_3 \ell_4 J\rangle \ . \qquad (22)$$

The angular part of the matrix element in the second term of equation (22) becomes:

$$\langle \ell_1 \ell_2 J|G\alpha\delta(\vec{r}_1-\vec{r}_2)|\ell_3 \ell_4 J\rangle = \frac{G\alpha}{4\pi}[\ell_1][\ell_2][\ell_3][\ell_4]\ x$$

$$\begin{pmatrix}\ell_1 & \ell_2 & J\\ 0 & 0 & 0\end{pmatrix}\begin{pmatrix}\ell_3 & \ell_4 & J\\ 0 & 0 & 0\end{pmatrix}. \qquad (23)$$

The strength of the spin-dependent term is proportional to α, and this parameter allows for a gradual degradation and eventual destruction of "pairing". Figure 2 shows how the spectrum is changed as α varies at constant G.

In our calculations we used the harmonic oscillator radial functions as defined in equation (24).

$$\Phi(r) = \sqrt{\frac{2n'!}{r_0^3\Gamma(n'+\ell+3/2)}}\left[\frac{r}{r_0}\right]^{\ell} e^{-r^2/2r^2} L_{n'}^{\ell+1/2}\left[\frac{r^2}{r_0^2}\right] \qquad (24)$$

The n' represents the principal quantum number, r_0 is the harmonic-oscillator well width and $L_j^i(x)$ is an associated Laguerre polynomial (7). By using this wave function, one can easily evaluate the radial matrix elements.

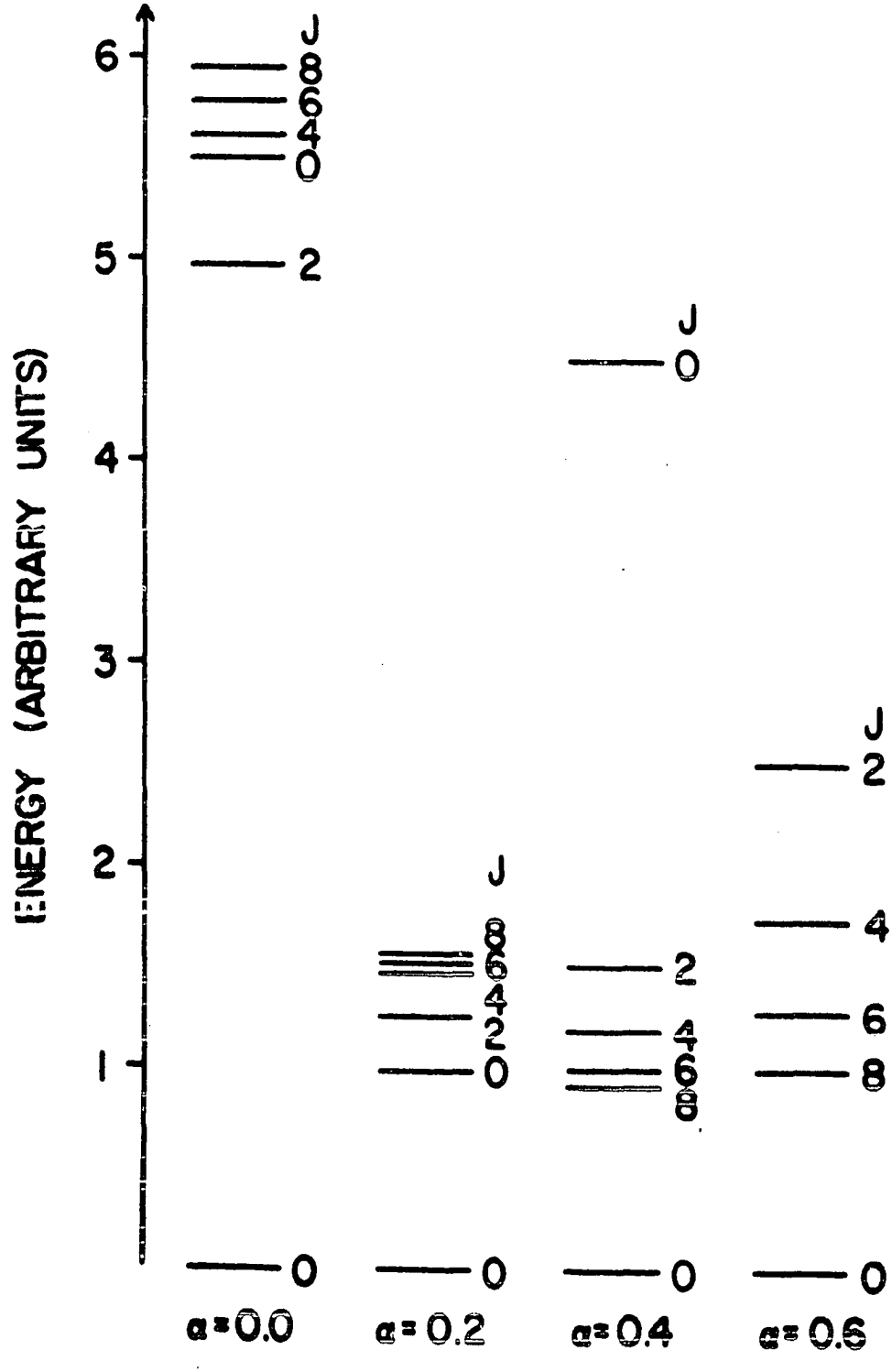

Figure 2. Eigenvalues of a spin-dependent interaction for the $(g_{9/2})^2(p_{1/2})^0$ and $(g_{9/2})^0(p_{1/2})^2$ configurations

For the Surface Delta Interaction, SDI, all interactions take place at the nuclear surface. The radial integral for a SDI is shown in equation (25).

$$\int dr_1 r_1^2 \int dr_2 r_2^2 \frac{\delta(R-r_1)\delta(R-r_2)}{r_1 r_2} \Phi_1(r_1)\Phi_2(r_2)\Phi_3(r_1)\Phi_4(r_2)$$

$$= R^2 \Phi_1(R)\Phi_2(R)\Phi_3(R)\Phi_4(R) \qquad (25)$$

The R in equation (25) is the nuclear radius, which must be defined or parameterized to evaluate the integral.

For a regular delta-force interaction between two particles, the nuclear radius does not need to be defined to evaluate the radial integral. The interactions will take place when the particles are "close" to each other, independent of the nuclear size. The radial integral for a normal delta interaction is given by equation (26).

$$\int dr_1 r_1^2 \, dr_2 r_2^2 \frac{\delta(r_1-r_2)}{r_1 r_2} \Phi_1(r_1)\Phi_2(r_2)\Phi_3(r_1)\Phi_4(r_2)$$

$$= \int r^2 dr \Phi_1(r)\Phi_2(r)\Phi_3(r)\Phi_4(r) \qquad (26)$$

A regular delta interaction was used in the course of these calculations because a reasonable definition of the nuclear radius involves an extra assumption or parameter for the calculation. In some calculations, this radial dependence is set constant, in the case of 1g and 2p radial integrals, the off-diagonal and both diagonal integrals are equal for the case where the nuclear radius is 1.364 times the well

width.

D. Five-Particle Calculation

The nucleus of ^{101}Tc is composed of 43 protons and 58 neutrons. It was assumed that the configuration of the extra-core neutrons is $(g_{7/2})^8$. This assumption is discussed in Appendix C. For the extra-core protons we assume $1g_{9/2}$ or $2p_{1/2}$ quantum numbers. These same proton configurations have been used successfully in calculations for ^{93}Tc by Vervier (2) and by Auerbach and Talmi (1). In order for other proton configurations to be of consequence, either a $p_{3/2}$ proton must be promoted to an outer shell, or a valence proton needs to jump to the $g_{7/2}$ orbital (see Figure 3). If our model is correct, the positive parity states can be described by the two configurations $(g_{9/2})^3(p_{1/2})^2$ and $(g_{9/2})^5(p_{1/2})^0$. It must be noted that the only way a negative-parity neutron state can be formed is by creating either a $p_{1/2}$ hole or an $h_{11/2}$ particle, both of which are extremely unlikely because of the energy needed for these excitations (see Figure 3). Therefore, we assume that all low-lying negative-parity states will come from the $(g_{9/2})^4(p_{1/2})^1$ proton configuration. This single-particle excitation should determine the separation of the $p_{1/2}$ and $g_{9/2}$ orbitals.

Our eigenvalue problem is developed in the following manner. We assume the eigenfunctions of H(SM) + V(residual)

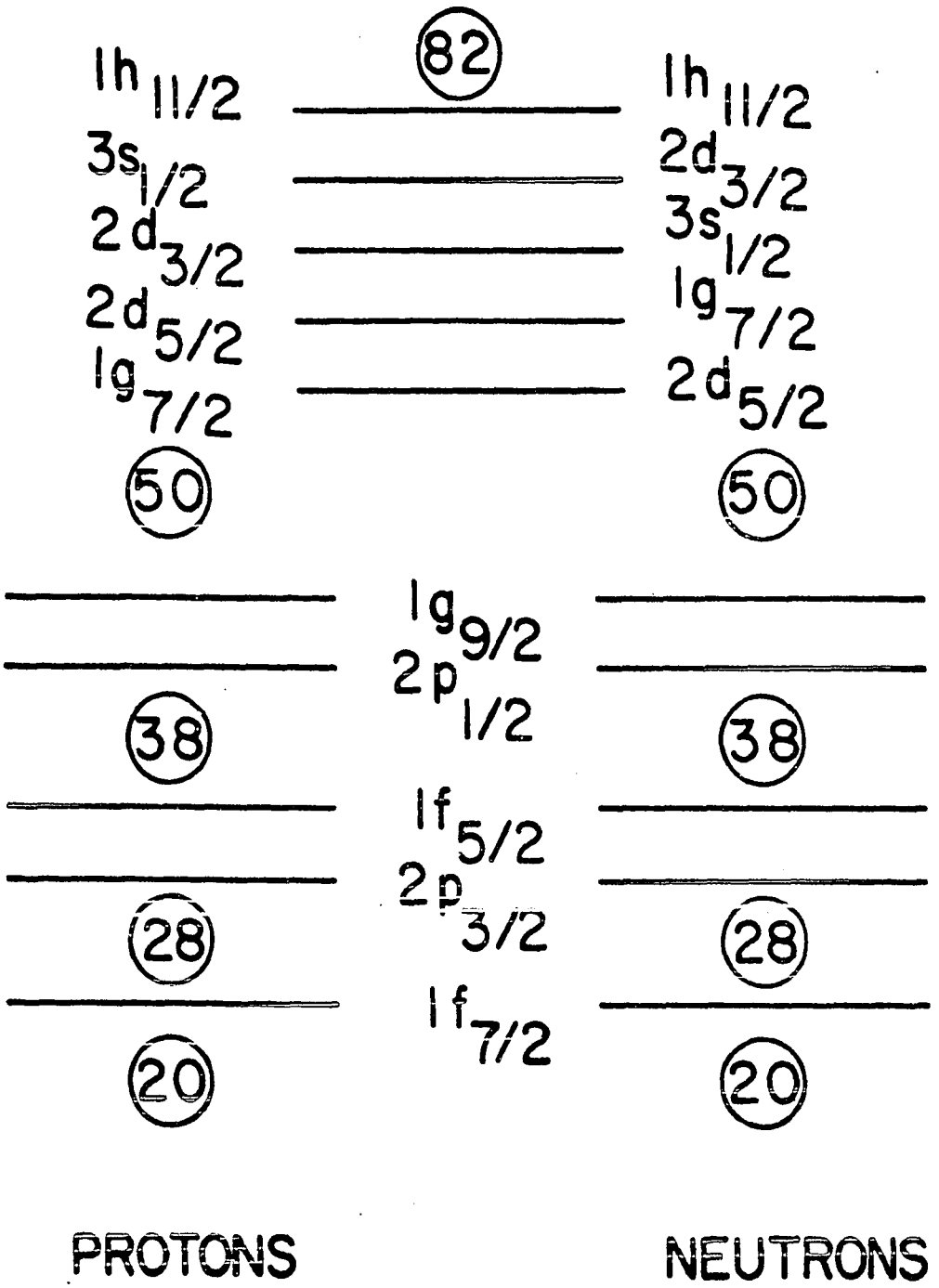

Figure 3. The ordering of shell-model eigenstates in the vicinity of ^{101}Tc

can be expanded in a series involving the configurations noted above. The accuracy of this assumption will be tested when we attempt to compare with experiment. The nuclear wave function is taken to be

$$|\alpha J> = \sum_i a_{i\alpha} |\phi_i> \qquad (27)$$

The coefficients $a_{i\alpha}$ are a measure of the pure 5-particle shell-model wave function $|\phi_i>$ (that describes the ith configuration) in the eigenstate $|\alpha J>$. Equation (28) is the matrix equation that must be diagonalized to determine the energy, $E_{\alpha J}$, of the state $|\alpha J>$ and the mixing coefficients $a_{i\alpha}$.

$$\sum_j (\varepsilon_i \delta_{ij} + <\phi_i|V|\phi_j>) \phi_{i\alpha} = E_{\alpha J} a_{i\alpha} \qquad (28)$$

The eigenvalues, ε_i, of the single-particle wave functions $|\phi_i>$ are the experimental single-particle energies of the states $|\phi_i>$. The V(residual) is the two-body residual interaction. Since the positive-parity states can be attained by two configurations, the off-diagonal and two diagonal matrix elements are needed. The negative-parity states are described by the diagonal matrix elements of the only configuration making those states. The matrix elements we need are $<(g_{9/2})^5(p_{1/2})^0|V|(g_{9/2})^5(p_{1/2})^0>$, $<(g_{9/2})^3(p_{1/2})^2|V|(g_{9/2})^3(p_{1/2})^2>$, $<(g_{9/2})^3(p_{1/2})^2|V|(g_{9/2})^5(p_{1/2})^0>$ and $<(g_{9/2})^4(p_{1/2})^1|V|(g_{9/2})^4(p_{1/2})^1>$.

The matrix element for two-body scalar operators between wave functions of n equivalent particles is given by equation (29). Since the energy of the nucleus is a scalar quantity, no other type of operator will be considered. Equivalent particles carry the same principal, orbital and total angular momentum quantum numbers.

$$\langle j^n \alpha J \mid \sum_{i<j} V_{\underline{i},\underline{j}} \mid j^n \alpha' J \rangle = \frac{n(n-1)}{2} \times \langle j^n \alpha J \mid V_{\underline{n},\underline{n-1}} \mid j^n \alpha' J \rangle \qquad (29)$$

Equation (30) is a result of combining equations (17) and (29).

$$\langle j_n \alpha J \mid \sum_{i<j} V_{\underline{ij}} \mid j^n \alpha' J \rangle = \frac{n(n-1)}{2} \sum_{\alpha_2 J_2 J_0} \times (j^{n-2}(\alpha_2 J_2) j^2(J_0); J \mid\} j^n \alpha J) \times (j^{n-2}(\alpha_2 J_2) j^2(J_0); J \mid\} j^n \alpha' J) \langle j^2 J_0 \mid V \mid j^2 J_0 \rangle \qquad (30)$$

The matrix element between two mixed-configuration wave functions is given by equation (31). A mixed-configuration is one for which all particles are not in the same orbital. In the ^{101}Tc calculation, the $(g_{9/2})^4(p_{1/2})^1$ and $(g_{9/2})^3(p_{1/2})^2$ are mixed configuration wave functions.

$$\langle j_1^{n_1}(\alpha_1 J_1) j_2^{n_2}(\alpha_2 J_2) J | \sum_{i<k} V_{\underline{ik}} | j_1^{n_1}(\alpha_1' J_1') j_2^{n_2}(\alpha_2' J_2') J \rangle =$$

$$\langle j_1^{n_1}\alpha_1 J_1 | \sum_{i<k}^{n_1} V_{\underline{ik}} | j_1^{n_1}\alpha_1' J_1' \rangle \, \delta_{J_1 J_1'} +$$

$$\langle j_2^{n_2}\alpha_2 J_2 | \sum_{i<k}^{n_2} V_{\underline{ik}} | j_2^{n_2}\alpha_2' J_2' \rangle \, \delta_{J_2 J_2'} +$$

$$\langle j_1^{n_1}(\alpha_1 J_1) j_2(\alpha_2 J_2) J | \sum_{i=1}^{n_1} \sum_{k=n_1+1}^{n_1+n_2} \times$$

$$| j_1^{n_1}(\alpha_1' J_1') j_2^{n_2}(\alpha_2' J_2') J \rangle \qquad (31)$$

The first two terms of equation (31) can be evaluated by using equation (30). The last term can be evaluated using Racah techniques (5) and is given by Equation 32.

The matrix element between a mixed configuration and a configuration involving equivalent particles can be calculated using the mixed-configuration wave function described in Appendix C. For our five-particle calculation, these matrix elements (8) are given by equation (33).

$$n_1 n_2 \sum_{\alpha_{11} J_{11}} \sum_{\alpha_{22} J_{22}} [J_1][J_1'][J_2][J_2'] \times$$

$$(j_1^{n_1-1}(\alpha_{11} J_{11}) j_1; J_1 | \} j_1^{n_1} \alpha_1 J_1) \times$$

$$(j_1^{n_1-1}(\alpha_{11} J_{11}) j_1; J_1 | \} j_1^{n_1} \alpha_1' J_1') \times$$

$$(j_2^{n_2-1}(\alpha_{22} J_{22}) j_2; J_2 | \} j_2^{n_2} \alpha_2 J_2) \times$$

$$(j_2^{n_2-1}(\alpha_{22} J_{22}) j_2; J_2 | \} j_2^{n_2} \alpha_2' J_2') \times$$

$$\sum_{J'} [J'] \langle j_1 j_2 J' | V_{\underline{n_1}, \underline{n_1+n_2}} | j_1 j_2 J' \rangle \times$$

$$\sum_{J_{12}} [J_{12}] \begin{Bmatrix} J_{11} & j_1 & J_1 \\ J_{22} & j_2 & J_2 \\ J_{12} & J' & J \end{Bmatrix} \begin{Bmatrix} J_{11} & j_1 & J_1' \\ J_{22} & j_2 & J_2' \\ J_{12} & J' & J \end{Bmatrix}. \qquad (32)$$

$$\langle j^5 \alpha J \mid \sum_{i<j} V_{\underline{ij}} \mid j_1^2(J_0'), j^3(\alpha_2' J_2'); \alpha' J \rangle = 10 \times$$

$$(j^3(\alpha_2' J) j^2(J_0'=0); J | \} j^5 \alpha J) \times$$

$$\langle j_1^2(J_0'=0) \mid V_{\underline{12}} \mid j^2(J_0'=0) \rangle \qquad (33)$$

In equation (33), $j=9/2$, $j_1=1/2$ and $J_2'=J$.

The calculation was performed using a FORTRAN program on the IBM 360/65 computer at the Iowa State University Computation Center. The calculations proceeded under the basic assumptions: 1) the single-particle energies are

parameters that represent the eigenvalues of the single-particle eigenfunctions; 2) a spin-dependent delta function is chosen to represent the two-body interaction that acts as a perturbation to the shell-model interaction; and 3) the true eigenfunction of the Hamiltonian can be expanded in a series involving the restricted basis. Some general results of the calculation are displayed in the next three figures.

Figure 4 shows the effect of varying the strength, α, of the spin-dependent term near 0.25. The trends in the eigenvalue behavior as this strength varies away from 0.25 can be extrapolated from Figure 4. As α increases from zero to 0.25, the positive-parity states decrease in energy from the delta interaction values to near the ground state while the negative-parity states proceed to their single-particle energies. It appears that in this range, the spin term softens the pairing interaction. When α increases from 0.25 to 1.0 the ordering of the negative-parity states changes to place the 5/2- level at a lower energy than that of the 1/2-. The positive-parity states are dispersed and the 5/2+ and 7/2+ levels increase in energy rapidly as α approaches the value 1.0.

Figure 5 illustrates the dependence of the eigenvalues on the strength of the pairing interaction, G. As G increases, the 1/2- state proceeds rapidly to below the

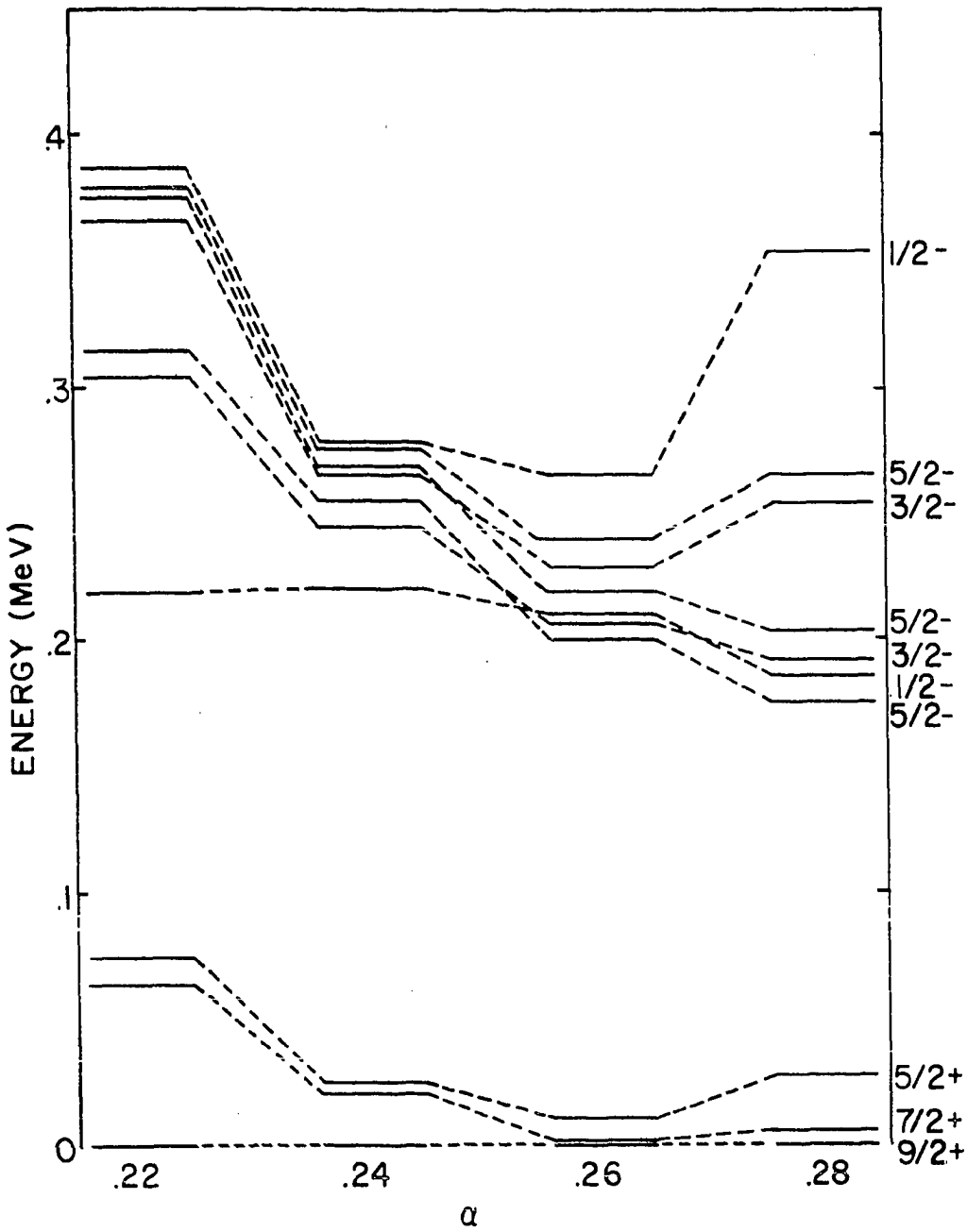

Figure 4. Some five-particle eigenvalues for $G=0.2$ MeV-r_0^3 and $\Delta\varepsilon=0.35$ MeV

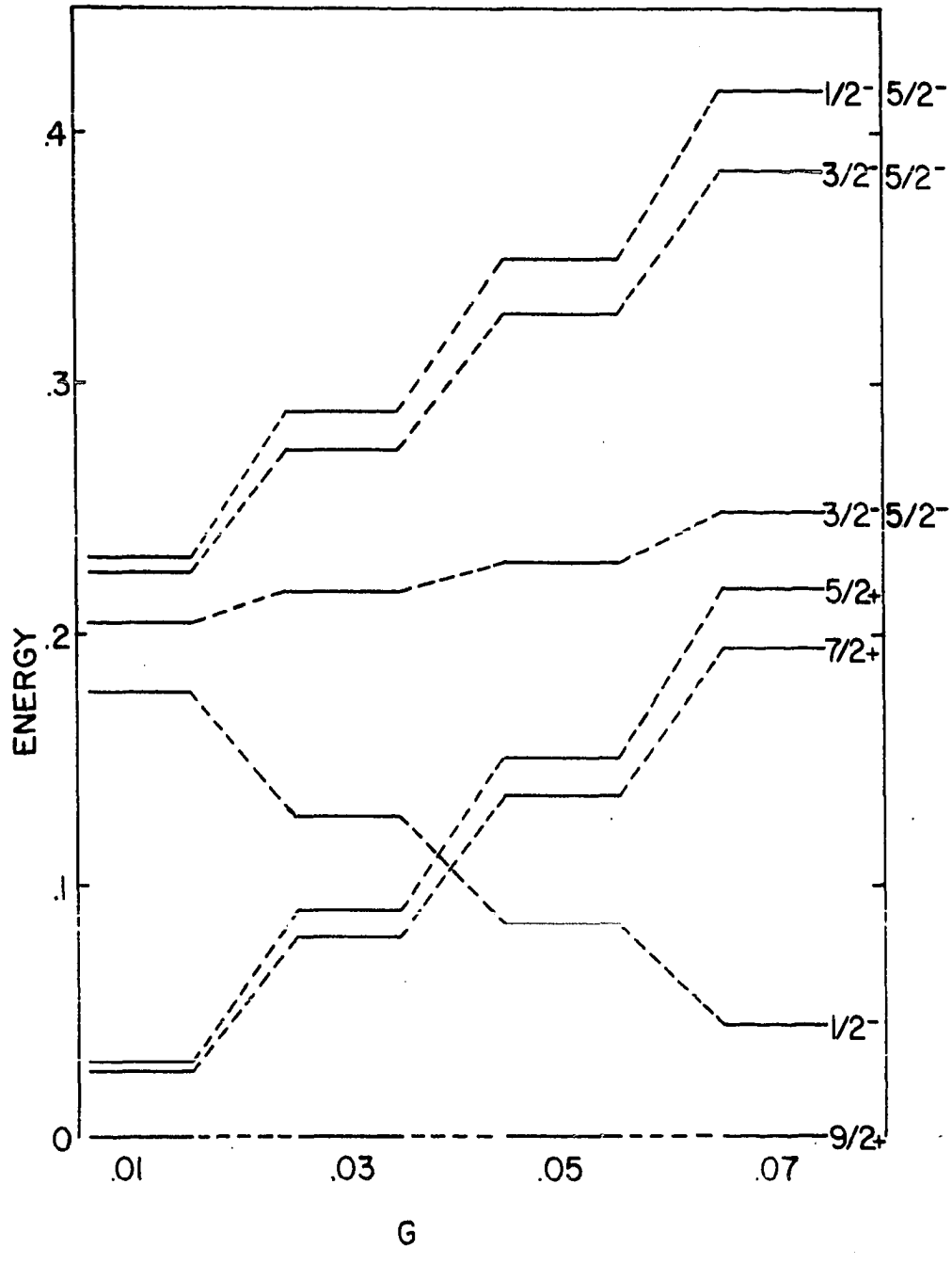

Figure 5. Some five-particle eigenvalues for $\Delta\varepsilon = 0.2$ MeV and $\alpha = 0.06$

ground state and the low-lying positive-parity states start climbing in energy, never to return to the close proximity of the ground state. When it appears that a particular level is falling or rising in Figures 4, 5 or 6, it is actually falling faster than, or falling slower than the ground state.

Figure 6 shows how the eigenvalues vary as the difference in single-particle energies is changed. This difference determines the separation between the negative- and positive-parity states since the negative-parity states are just hole states, or single-particle excitations, of the positive-parity states. It should be noted that all calculated levels are not included in Figures 4, 5 and 6 which serve only to show general trends and not the locations of specific eigenvalues.

Auerbach and Talmi (1) used effective interaction methods to calculate the ground-state wave function of ^{93}Tc. The results of their calculation give a separation of 0.794 MeV for the $2p_{1/2}$ and $1g_{9/2}$ single-particle energy levels. Their two-body, seniority-zero matrix element was calculated to be 1.774 MeV. In this work, the spin-dependent, two-body seniority-zero matrix element was calculated to be 1.8 MeV for $\alpha = 0.33$ and with the radial integral normalized to unity. The inability of the single-particle energy differences and two-body matrix elements of the A=93

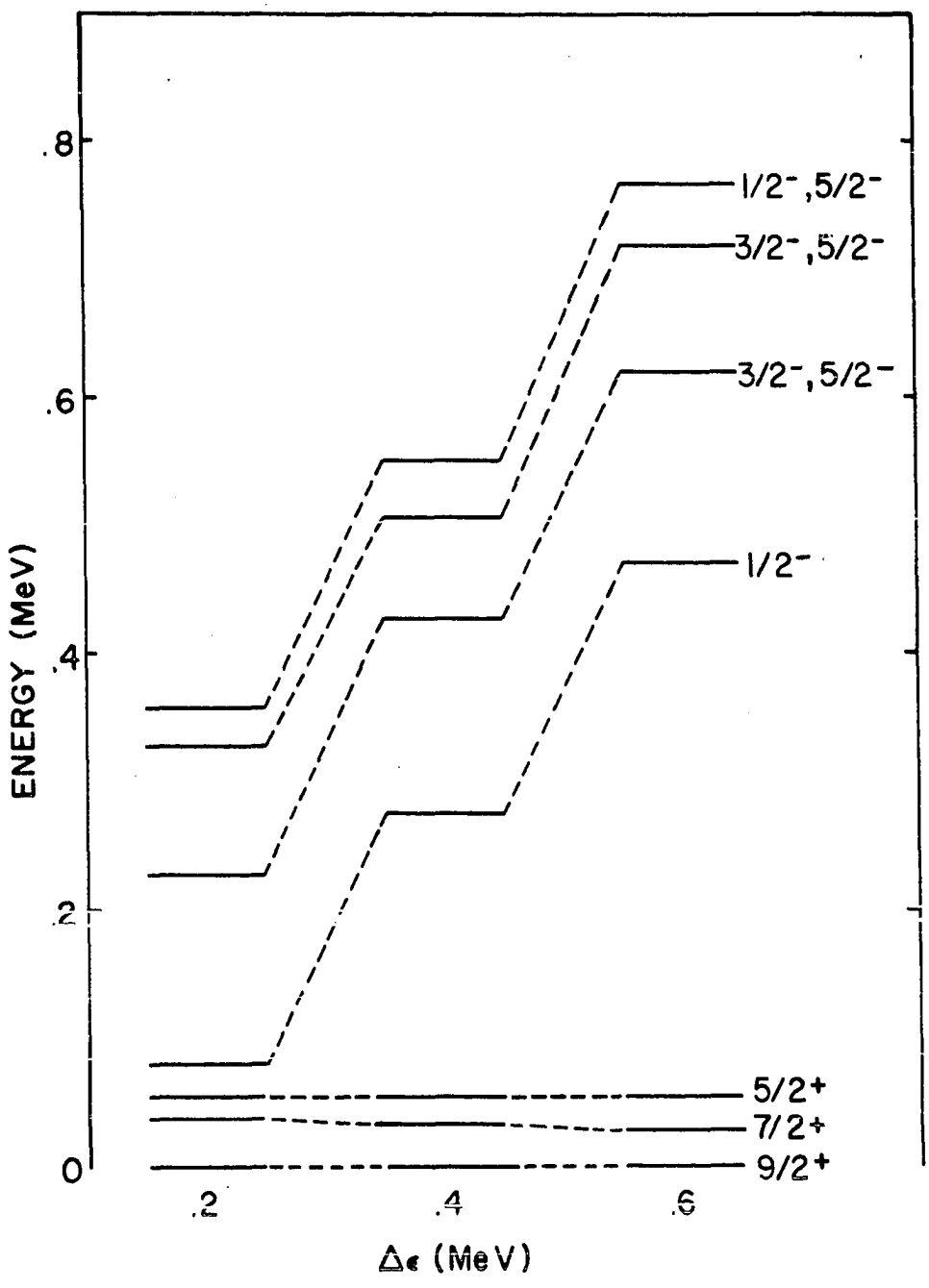

Figure 6. Some five-particle eigenvalues for $\alpha=0.06$ and $G=0.05$ MeV-r_0^3

calculation to give comparable results for the A=101 case is probably due to the differences in the methods of calculation. This work is more constrained in that the negative-parity calculation was directly coupled to the positive-parity calculation, while Auerbach and Talmi treated states of different parity as separate problems.

The energy levels of ^{101}Tc with experimentally determined spins and parities are the 9/2+, 7/2+, 5/2+ and 1/2- states at 0.00, 9.36, 15.58 and 207.51 keV, respectively. Calculations were performed for many ranges of α,G and $\Delta\varepsilon$. The eigenvalues that best fit the low-lying experimental levels are given in Table 1. Table 1 gives a comparison of the low-energy eigenvalues with the low-lying experimentally observed levels. The mixing coefficients for the resulting eigenfunctions are given in Table 2. One of the main difficulties apparent in Table 1 is that not enough high-spin states are seen in the low-energy experimental level scheme. Another major difference is that several levels seen experimentally below 1.0 MeV (see Figure 8) have possible spin-parity assignments of 3/2± or 5/2-. The configurations used in this calculation can only give two 3/2+ states, two 3/2- states and three 5/2- states. More of these states could be obtained by increasing the size of the configuration space to include single-particle excitations from the $f_{5/2}$ shell such as $(f_{5/2})^5(g_{9/2})^6(p_{1/2})^2$ and

Table 1. Eigenvalues for five-particle calculation

Calculated J	Calculated E(keV)	Experimental J	Experimental E(keV)	Calculated J	Calculated E(keV)	Experimental J	Experimental E(keV)
9/2+	0	9/2+	0	7/2-	232		
7/2+	12	7/2+	9	9/2-	232		
5/2+	14	5/2+	16	11/2-	232		
13/2+	14			13/2-	233		
11/2+	15			19/2-	233		
9/2+	18			17/2-	233		
15/2+	19			17/2-	234		
17/2+	19			19/2-	235		
21/2+	20			21/2-	241		
3/2+	22			23/2-	242		
1/2-	207	1/2-	207	25/2-	242	3/2-	288
3/2-	220			9/2+	433		395
5/2-	220			7/2+	442		
7/2-	222			5/2+	444		
9/2-	223			13/2+	444		
11/2-	223			11/2+	444		
15/2-	223			9/2+	445		
13/2-	224			15/2+	447		
17/2-	224			17/2+	447		
7/2-	228			5/2+	447		
9/2-	229			21/2+	448		
3/2-	229			11/2+	449		
11/2-	230			17/2+	451		
5/2-	230			7/2+	451		
13/2-	230			15/2+	451		
9/2-	231			9/2+	451		
13/2-	231			13/2+	452		
11/2-	231			3/2+	455		
7/2-	231			1/2+	456		
5/2-	231			19/2+	460		
1/2-	232			25/2+	463		
15/2-	232						

Table 2. Mixing coefficients

Energy (keV)	J^{π}	$\|(9/2)^5(1/2)^0\rangle$			$\|(9/2)^4(1/2)^1\rangle$			$\|(9/2)^3(1/2)^2\rangle$	
		$\nu=1$	$\nu=1$	$\nu=5$	$\nu=1$	$\nu=3$	$\nu=5$	$\nu=1$	$\nu=3$
0	9/2+	-0.012	-0.003	0.0				0.917	0.398
12	7/2+		-0.008	0.0					0.999
14	5/2+		-0.008	0.0					0.999
22	3/2+		0.012						0.998
207	1/2-				1.000		0.0		
220	3/2-					1.000	0.0		
229	3/2-					0.0	1.000		
232	1/2-				0.0		1.000		
455	3/2+		0.998						-0.012

$(f_{5/2})^5(g_{9/2})^7(p_{1/2})^1$.

In conclusion, it should be noted that even though the calculation gives a high density of low-energy states that could be populated by gamma decay but are not seen experimentally, this spin-dependent potential calculation does indicate one manner in which the 7/2+ and 5/2+ levels can be located near the ground state.

II. NUCLEAR DECAYS OF ^{101}Mo AND ^{101}Tc

A. Introduction

The decay of ^{101}Mo has been the subject of several independent studies in the past two years(9-12). The low-lying positive-parity states in ^{101}Tc are of particular interest to the nuclear spectroscopist(13), and are thought to be similar to the anomalous states of the odd Ge and Ag isotopes (14). The anomaly in odd-A Tc isotopes is characterized by the lowering of the 7/2+ and 5/2+ states with respect to the 1/2- level as pairs of neutrons are added to the nucleus. The lifetimes of the metastable states in these nuclei have also been measured. The 1/2- state at 207 keV in ^{101}Tc has a reported half-life of 760 sec (15). The half-life for the 127-keV level in ^{101}Ru is measured to be 580 nsec (16). When this study was started, the existing decay schemes of ^{101}Mo and ^{101}Tc were inconsistent and incomplete. This work was undertaken in an attempt to resolve these discrepancies and to better understand the trends in nuclear structure for this region of nuclei.

B. Experimental Procedure

Natural molybdenum has an isotopic distribution (17) of 9.62% ^{100}Mo, 23.75% ^{99}Mo, 9.45% ^{97}Mo, 16.50% ^{96}Mo, 15.70% ^{95}Mo, 9.12% ^{94} and 15.86% ^{92}Mo. The products of neutron

capture from natural Molybdenum are $^{93}Mo(T_{1/2} > 100$ years), ^{99}Mo ($T_{1/2}$ = 67 hours) and ^{101}Mo ($T_{1/2}$ = 14.62 minutes). The decay of ^{99}Mo exhibits gamma rays connecting known levels in ^{99}Tc. The daughter, ^{99}Tc, ($T_{1/2}$ = 2.12 X 10^5 years) decays by beta emission to the ground state of ^{99}Ru. ^{101}Mo decays by beta emission to ^{101}Tc ($T_{1/2}$ = 14.2 minutes), which in turn decays by beta emission to the stable ^{101}Ru. The cross section for the $^{98}Mo(n,\gamma)^{99}Mo$ reaction is 0.51 b, compared to that for $^{100}Mo(n,\gamma)^{101}Mo$ of 0.2 b. It was decided that a short-term irradiation of natural molybdenum would produce sufficient and interference free activity for the determination of the decay schemes of ^{101}Mo and ^{101}Tc.

Sources of electron beam melted Mo metal, and high purity MoO_3, were irradiated in the 5 Megawatt Ames Laboratory Research Reactor (ALRR) fast transit irradiation facility. The irradiations were for 5 sec and at a neutron flux of 1.2 X 10^{13} neutrons/cm^2 - sec. The Tc and Mo were separated chemically in the TcO_4^{-2} and the MoO_4^{-2} forms (18). The irradiated sample of 500 mg MoO_3 was dissolved in 10 ml of 0.5N NaOH and 5ml of 14.8N NH_4OH. The Tc was extracted using 50 mg $(C_6H_5)_4AsCl$ and 10 ml $HCCl_3$. A continuous separation was performed by placing the aqueous and organic phases in a beaker with a magnetic stirrer. By controlling the solid angle the detector had with the layers

of liquid, one could look at either the daughter decay or predominantly parent decay.

Singles gamma-ray measurements were made using Ge(Li) detectors over an energy range sufficient to give the gamma-ray spectrum up to the total beta decay energy, or Q-value, of each isotope. The Q-values for the ^{101}Mo and ^{101}Tc decay are 2.84 ± 0.04 and 1.63 ± 0.03 MeV, respectively. The calibration sources and a block diagram of the electronics are given in Appendix B. Figure 7 gives the gamma-ray spectrum of the ^{101}Tc decay in equilibrium with the ^{101}Mo activity.

Coincidence spectra of equilibrium samples were collected with the 4096 X 4096 two-parameter system (Appendix B) at the TRISTAN facility. Constant fraction timing units were used to determine detection times for the gamma rays, and an acceptance gate of 35 nsec was used in the coincidence circuit.

C. Data Analysis

The location and area of each peak in the equilibrium spectrum were determined with the program SKEWGAUS (Appendix A). These locations and areas were fed to the program DRUDGE (Appendix A) to give the energies and relative intensities of the photopeaks. The spectrum of the chemically separated activity was used to make decay assignments. The peak areas determined for the chemically

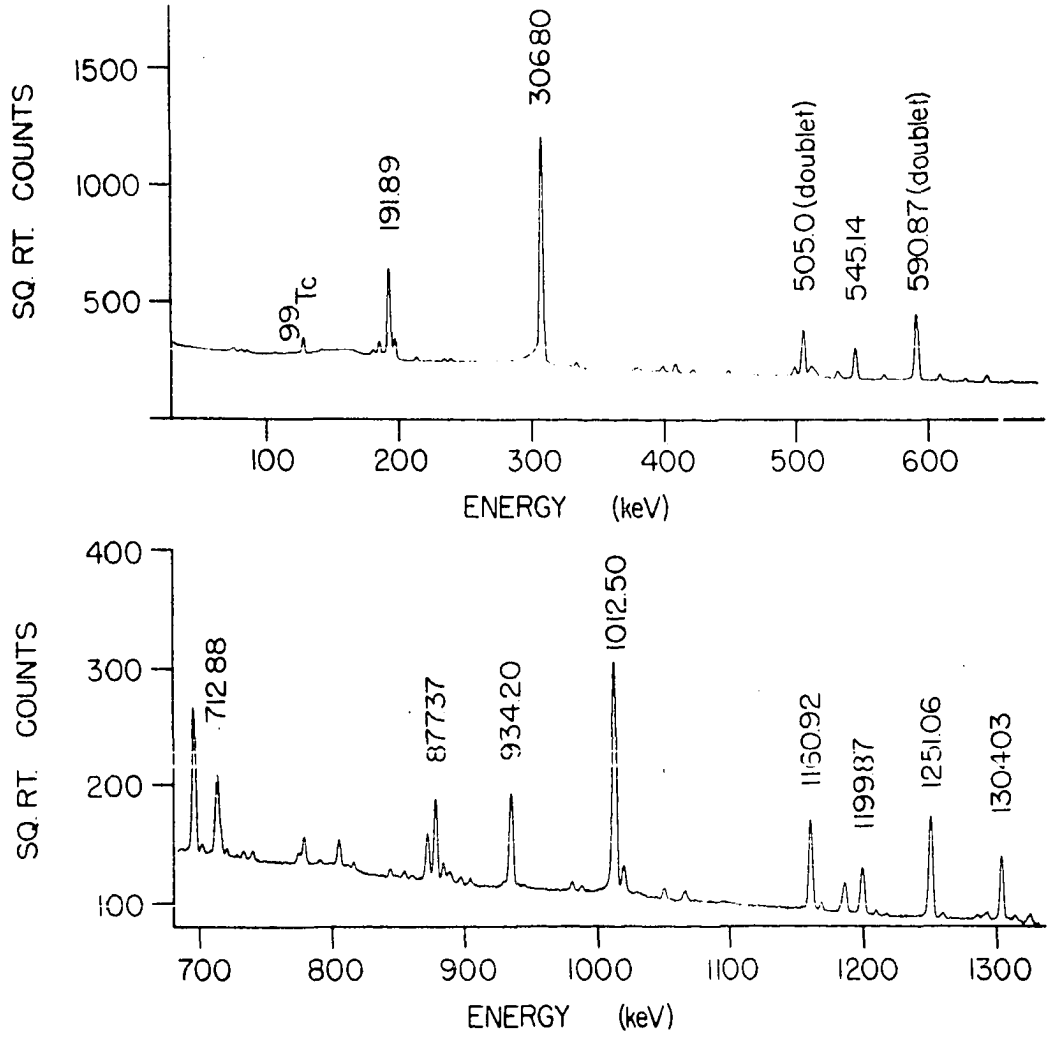

Figure 7. **The gamma-ray spectrum for the equilibrium decay of ^{101}Mo and ^{101}Tc**

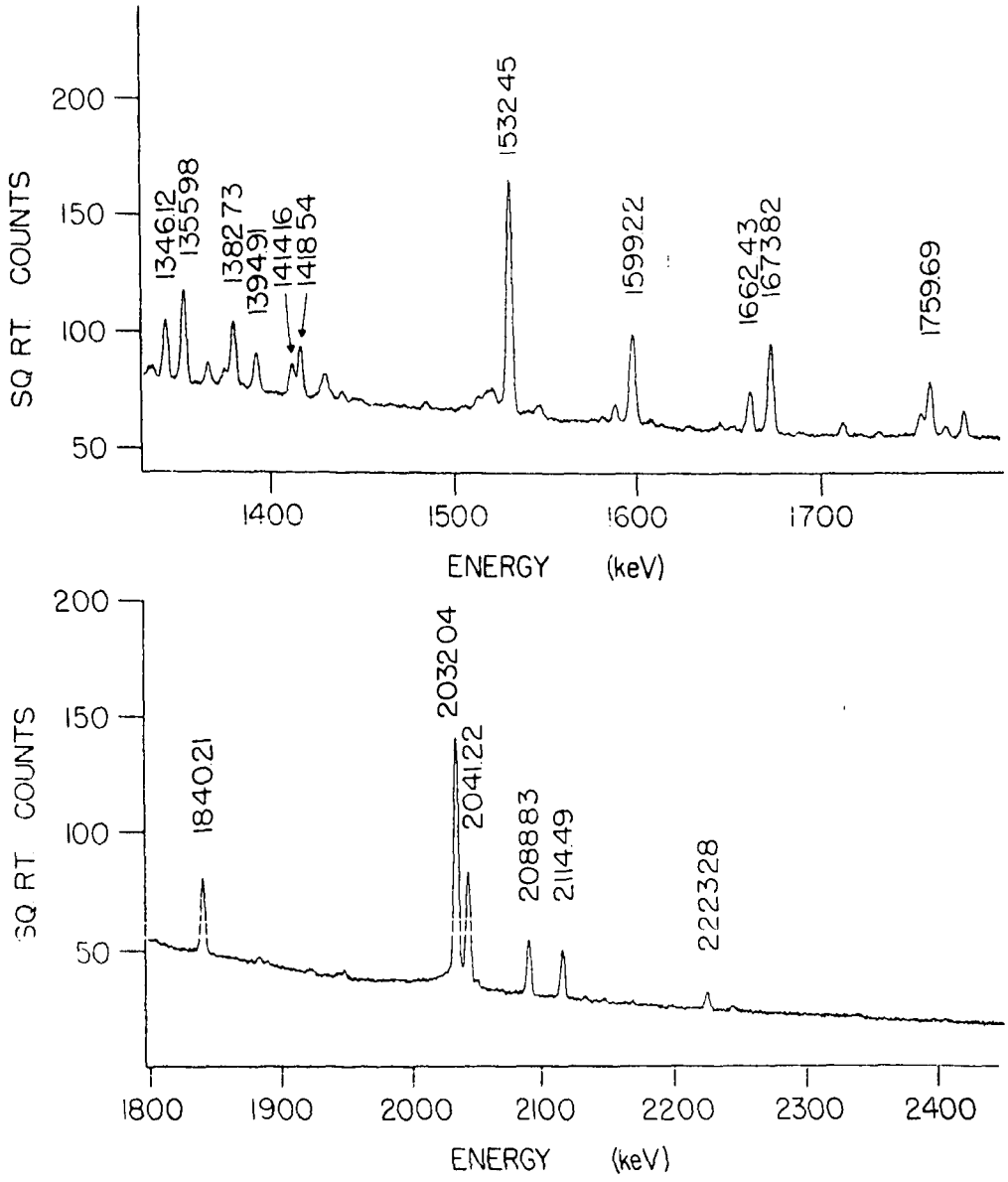

Figure 7. (continued)

separated spectrum were compared with the peak areas of an equilibrium decay. The assignment of a peak to either the ^{101}Mo decay, the ^{101}Tc decay or both decays was done on the basis of these comparisons. The gamma rays assigned to the ^{101}Mo and ^{101}Tc decays are listed in Tables 3 and 4, respectively.

The coincidence data were analyzed by visually comparing the gamma-ray spectrum in coincidence with each gating peak to the gamma-ray spectrum in coincidence with the background of the gating peak (see Appendix B). The results of the coincidence experiments are given in Tables 5 and 6.

D. Results

The construction of experimental level schemes must proceed with some definite rules. The gamma-ray energies are used by the program LVLSURCH to construct a possible level scheme which is presented along with a summary of coincidence information. However, a need exists to determine the viability of a particular level in this scheme. A confidence index (CI) can be established to indicate this viability. The CI is defined as twice the sum of all gamma rays entering and leaving the level that are verified by coincidence information, plus the sum of all gamma rays entering or leaving the level. Any level with a CI < 4 has been indicated as a dashed line in the level

Table 3. Gamma-ray transitions in ^{101}Tc

Energy (keV)	Relative[1] Intensity	Assignment
80.67(0.14)	281.29(21.18)	288. -> 208.
105.52(0.36)	27.62(13.84)	
115.57(0.28)	8.78(2.23)	616. -> 500.
187.41(0.20)	25.45(4.63)	395. -> 208.
188.20(0.50)	300.84(120.3)	1806. -> 1618.
191.89(0.05)	1000.00(51.38)	208. -> 16.
195.90(0.07)	152.17(9.21)	711. -> 515.
211.88(0.08)	27.20(1.74)	500. -> 288.
221.80(0.23)	5.29(1.14)	742. -> 520.
274.93(0.21)	4.81(1.02)	670. -> 395.
292.03(0.50)	13.24(6.02)	1320. -> 1028.
317.77(0.13)	12.52(1.44)	1962. -> 1644.
327.68(0.13)	11.31(1.32)	616. -> 288.
333.50(0.07)	41.28(2.41)	622. -> 288.
367.91(0.65)	5.66(3.19)	1962. -> 1594.
347.30(0.24)	5.23(1.02)	1962. -> 1615.
352.90(0.17)	7.52(1.14)	887. -> 533.
358.22(0.49)	2.47(1.38)	1678. -> 1319.
369.95(0.76)	8.30(4.51)	2048. -> 1678.
371.55(0.82)	8.24(4.87)	887. -> 515.
377.90(0.54)	8.72(4.39)	911. -> 533.
379.29(0.34)	17.21(4.87)	395. -> 16.
381.23(0.14)	16.19(1.81)	670. -> 288.
384.26(0.50)	0.12(0.06)	
398.70(0.07)	47.89(2.77)	606. -> 207.
408.53(0.06)	85.02(4.75)	616. -> 207.
421.84(0.24)	21.96(8.54)	1028. -> 606.
441.97(0.38)	2.65(0.96)	2057. -> 1615.
448.49(0.06)	36.70(2.05)	2048. -> 1599.
452.37(0.27)	3.85(0.96)	1122. -> 670.
469.04(0.22)	6.20(1.14)	
491.38(0.32)	3.73(0.84)	500. -> 9.
497.02(0.80)	7.10(4.69)	1103. -> 606.
499.19(0.34)	71.12(26.41)	515. -> 16.
505.05(0.18)	176.41(67.15)	521. -> 16.
505.93(0.08)	517.93(71.66)	515. -> 9.

[1]Relative to 191.89 keV transition and multiply by 0.01932 for transitions/100 decays

Table 3. (continued)

Energy (keV)	Relative[1] Intensity	Assignment
510.14(0.14)	52.41(5.90)	2558. -> 2048.
512.18(0.17)	93.20(8.00)	1028. -> 515.
514.06(0.39)	43.08(6.38)	1618. -> 1103.
515.80(0.25)	27.32(6.62)	1122. -> 606.
523.80(0.12)	9.21(1.14)	533. -> 9.
533.51(0.11)	21.30(1.87)	533. -> 0.
540.10(0.52)	4.99(3.31)	2218. -> 1678.
560.25(0.34)	3.73(0.84)	2238. -> 1678.
566.65(0.19)	38.63(12.52)	1594. -> 1028.
571.69(0.19)	9.93(1.26)	1188. -> 616.
582.85(0.86)	4.81(2.59)	1103. -> 521.
590.10(0.19)	304.21(145.1)	1618. -> 1028.
590.87(0.08)	872.02(151.3)	606. -> 16.
602.98(0.24)	5.35(1.26)	1103. -> 500.
606.76(0.32)	11.25(3.61)	616. -> 9.
608.32(0.08)	56.68(4.51)	1320. -> 711.
611.55(0.45)	7.70(3.13)	2573. -> 1962.
625.60(0.46)	5.48(3.49)	1232. -> 606.
642.58(0.05)	66.06(3.67)	1962. -> 1320.
650.55(1.06)	1.50(1.08)	1678. -> 1028.
652.66(1.12)	1.50(1.08)	1775. -> 1122.
660.61(0.10)	11.91(0.90)	670. -> 9.
675.91(0.56)	2.47(1.02)	2573. -> 1898.
686.02(0.32)	3.55(1.02)	1808. -> 1122.
695.60(0.09)	309.03(49.04)	711. -> 16.
701.80(0.13)	17.63(2.29)	711. -> 9.
707.80(0.78)	3.43(1.74)	1594. -> 887.
712.88(0.06)	173.83(9.27)	1320. -> 606.
727.94(0.28)	4.93(1.62)	2048. -> 1320.
732.92(0.25)	13.90(3.79)	742. -> 9.
737.33(0.75)	2.47(1.32)	2057. -> 1319.
739.54(0.13)	16.00(1.50)	1028. -> 288.
773.81(0.17)	17.81(2.47)	
775.79(0.76)	5.66(1.87)	1898. -> 1122.
778.17(0.08)	51.26(3.01)	1806. -> 1028.
790.01(0.18)	6.74(0.96)	
797.99(0.48)	3.79(1.14)	2573. -> 1775.
804.19(0.08)	52.65(2.95)	1320. -> 515.
815.20(0.18)	9.45(1.38)	1103. -> 288.
847.27(0.25)	4.45(0.84)	2442. -> 1594.

Table 3. (continued)

Energy (keV)	Relative[1] Intensity	Assignment
852.98(0.11)	12.39(1.02)	2659. -> 1806.
859.09(0.19)	5.90(0.90)	1962. -> 1103.
869.72(0.30)	17.63(5.90)	1898. -> 1028.
871.11(0.10)	82.31(7.28)	887. -> 16.
877.37(0.09)	164.02(14.86)	887. -> 9.
883.31(0.09)	33.45(2.11)	1594. -> 711.
886.97(0.28)	12.27(2.95)	887. -> 0.
888.74(0.29)	12.15(2.71)	1775. -> 887.
894.36(1.56)	3.13(2.59)	1806. -> 911.
896.31(0.41)	11.31(3.01)	1103. -> 207.
903.41(0.15)	10.65(1.20)	1615. -> 711.
933.28(0.31)	40.07(24.01)	1644. -> 711.
934.20(0.11)	181.05(25.75)	1962. -> 1028.
943.51(0.27)	4.81(1.26)	1232. -> 288.
980.40(0.12)	14.08(1.14)	1188. -> 207.
987.94(0.17)	8.36(1.14)	1594. -> 606.
1007.38(0.30)	9.39(1.56)	2130. -> 1122.
1011.05(0.14)	119.55(18.95)	1618. -> 606.
1012.50(0.08)	683.03(39.05)	1028. -> 15.
1018.58(0.25)	34.12(10.11)	1028. -> 9.
1019.97(0.34)	24.55(10.05)	2048. -> 1028.
1030.06(0.40)	3.79(1.08)	2218. -> 1188.
1049.75(0.10)	18.41(1.20)	2238. -> 1188.
1064.22(0.32)	11.43(3.31)	1775. -> 711.
1065.88(0.41)	8.60(3.31)	1599. -> 533.
1160.92(0.09)	211.25(10.77)	2048. -> 887.
1168.99(0.17)	12.45(1.38)	1775. -> 606.
1184.19(0.23)	10.35(1.44)	1806. -> 622.
1186.59(0.09)	54.51(3.07)	1898. -> 711.
1199.87(0.08)	93.26(4.87)	1806. -> 606.
1209.88(0.22)	7.04(1.02)	2238. -> 1028.
1218.03(0.50)	2.95(1.08)	2130. -> 911.
1249.37(0.46)	14.20(6.50)	1644. -> 395.
1251.06(0.08)	244.77(14.02)	1962. -> 711.
1260.53(0.29)	8.06(1.62)	1775. -> 515.
1286.26(0.17)	7.64(0.72)	
1290.69(0.30)	6.08(0.96)	1806. -> 515.
1293.29(0.17)	11.13(1.08)	1808. -> 515.
1304.03(0.09)	148.07(7.64)	1320. -> 16.
1308.22(0.73)	4.99(1.93)	1808. -> 500.

Table 3. (continued)

Energy (keV)	Relative[1] Intensity	Assignment
1310.70(1.25)	3.07(1.81)	1599. -> 288.
1314.28(0.25)	12.33(1.44)	2057. -> 742.
1325.78(0.32)	13.72(4.57)	2558. -> 1232.
1336.64(0.26)	7.40(1.20)	2048. -> 711.
1339.36(0.20)	9.27(1.20)	2659. -> 1319.
1346.12(0.11)	55.90(4.75)	1962. -> 616.
1350.78(0.65)	2.23(0.84)	2238. -> 887.
1355.99(0.11)	89.35(9.09)	1962. -> 606.
1377.72(0.20)	13.00(1.50)	2048. -> 670.
1380.43(0.79)	5.66(1.74)	1775. -> 395.
1382.73(0.10)	61.25(3.79)	1898. -> 515.
1387.63(0.32)	4.15(0.84)	2130. -> 742.
1394.91(0.13)	32.37(2.65)	2001. -> 606.
1414.16(0.10)	26.65(1.62)	2442. -> 1028.
1418.54(0.09)	46.57(2.59)	2130. -> 711.
1426.86(0.88)	1.87(0.84)	2659. -> 1232.
1429.99(0.60)	7.28(2.53)	
1432.05(0.25)	19.13(2.65)	2048. -> 616.
1435.05(0.39)	4.69(1.02)	2057. -> 622.
1440.85(0.15)	8.42(0.72)	2048. -> 606.
1451.12(0.36)	3.49(0.66)	2573. -> 1122.
1485.92(0.21)	5.48(0.78)	2001. -> 515.
1507.00(0.73)	2.11(1.08)	2218. -> 711.
1514.10(0.22)	9.93(1.14)	2048. -> 533.
1517.80(0.35)	11.73(2.17)	1806. -> 288.
1520.39(0.50)	12.45(1.99)	1808. -> 288.
1522.95(0.30)	15.40(2.29)	2130. -> 606.
1526.57(0.47)	5.96(1.14)	2238. -> 711.
1530.34(0.45)	14.56(4.51)	2558. -> 1028.
1532.45(0.08)	317.09(16.67)	2048. -> 515.
1548.68(0.24)	8.00(1.26)	2218. -> 670.
1583.11(0.27)	4.45(0.60)	1599. -> 16.
1589.61(0.12)	14.98(1.02)	1599. -> 9.
1594.84(0.88)	1.56(0.72)	1594. -> 0.
1599.22(0.08)	93.08(4.75)	1615. -> 16.
1605.31(0.57)	2.41(0.66)	1615. -> 9.
1609.16(0.27)	5.23(0.78)	2130. -> 521.
1614.96(0.39)	3.13(0.66)	1615. -> 0.
1629.40(0.51)	2.89(1.08)	2130. -> 500.

Table 3. (continued)

Energy (keV)	Relative[1] Intensity	Assignment
1646.38(0.34)	4.09(0.90)	2558. -> 911.
1653.29(0.41)	3.31(0.84)	2048. -> 395.
1662.43(0.09)	36.40(2.05)	1678. -> 16.
1673.81(0.08)	89.83(4.63)	1962. -> 288.
1712.76(0.17)	10.65(1.14)	2001. -> 288.
1722.06(0.61)	1.68(0.72)	2238. -> 515.
1754.84(0.12)	18.47(1.26)	1962. -> 207.
1759.69(0.09)	52.11(2.77)	1775. -> 15.
1768.22(0.19)	7.88(0.84)	2057. -> 288.
1840.21(0.09)	73.04(3.79)	2048. -> 207.
1876.25(0.89)	1.26(0.84)	
1882.26(0.25)	4.75(0.90)	1898. -> 16.
1888.27(0.50)	2.23(1.20)	1898. -> 9.
1921.35(0.54)	2.05(0.72)	2442. -> 520.
1941.75(0.40)	2.89(0.66)	2558. -> 616.
1946.54(0.24)	4.99(0.72)	1962. -> 16.
2024.41(0.78)	4.03(1.44)	2558. -> 533.
2028.11(0.87)	5.48(1.81)	
2032.04(0.10)	368.65(18.89)	2048. -> 16.
2038.38(0.45)	11.43(2.83)	2048. -> 9.
2041.22(0.11)	111.91(6.50)	2057. -> 15.
2047.67(0.48)	4.69(1.14)	2048. -> 0.
2088.82(0.12)	52.23(2.77)	
2112.77(0.25)	7.94(2.77)	
2114.49(0.16)	24.13(2.11)	2130. -> 16.
2131.36(0.36)	1.87(0.36)	
2223.28(0.14)	8.84(0.66)	
2337.78(0.75)	0.90(0.42)	
2404.74(0.79)	0.78(0.36)	

Table 4. Gamma-ray transitions in ^{101}Ru

Energy (keV)	Relative[1] Intensity	Assignment
127.16(0.10)	31.09(1.63)	127. -> 0.
179.74(0.20)	6.96(1.11)	307. -> 127.
184.30(0.09)	18.35(1.32)	311. -> 127.
233.69(0.09)	2.98(0.23)	545. -> 311.
238.21(0.09)	3.33(0.25)	545. -> 307.
281.60(0.66)	0.30(0.18)	1002. -> 720.
294.75(0.50)	0.30(0.15)	422. -> 127.
306.80(0.06)	1000.00(57.80)	307. -> 0.
311.50(0.34)	1.51(0.48)	311. -> 0.
384.26(0.50)	0.43(0.24)	929. -> 545.
393.33(0.17)	1.49(0.30)	939. -> 545.
421.84(0.24)	0.80(0.35)	422. -> 0.
515.80(0.25)	1.18(0.36)	939. -> 422.
531.53(0.07)	11.14(0.62)	843. -> 311.
545.14(0.06)	64.71(3.31)	545. -> 0.
617.47(0.27)	0.56(0.11)	929. -> 311.
622.43(0.18)	0.97(0.14)	929. -> 307.
627.12(0.13)	4.23(0.46)	939. -> 311.
631.89(0.33)	0.45(0.11)	939. -> 307.
673.39(0.61)	0.41(0.18)	
694.73(0.28)	12.62(7.73)	1002. -> 307.
715.52(0.11)	7.48(0.57)	843. -> 127.
720.09(0.25)	1.84(0.31)	720. -> 0.
810.26(0.58)	0.52(0.19)	939. -> 127.
842.79(0.10)	2.50(0.20)	843. -> 0.
928.61(0.18)	1.38(0.23)	929. -> 0.
938.87(0.24)	0.95(0.18)	939. -> 0.

[1]Relative to 306.80 keV transition and multiply by 0.0905 for transitions/100 decays

Table 5. Gamma-ray coincidences in ^{101}Tc

Gate (keV)	Coincidences (keV)
195	505,499,1186,1251
408	1346
499	195,512,934,1251,1532
505	195,804,1251,1382,1414,1532
512	499,505,934
566	1012
590	712,1199,1355,1395
608	195,695
642	1304
695	883,1186,1251,1418
701	1251
712	590
778	1012
804	505
877	1160
883	695
888	877
903	695
934	1012
1012	292,566,590,934,1019
1020	1012
1160	871,877
1186	195,695
1199	590
1251	195,505,499,695,702
1304	642
1346	408
1356	590
1382	505
1394	590
1414	505,512
1418	195,695
1532	505,499

Table 6. Gamma-ray coincidences in ^{101}Ru

Gate (keV)	Coincidences (keV)
127	180,184,531,715
184	127,234,531
294	127
306	238,694
531	127.184.311
694	307
715	127

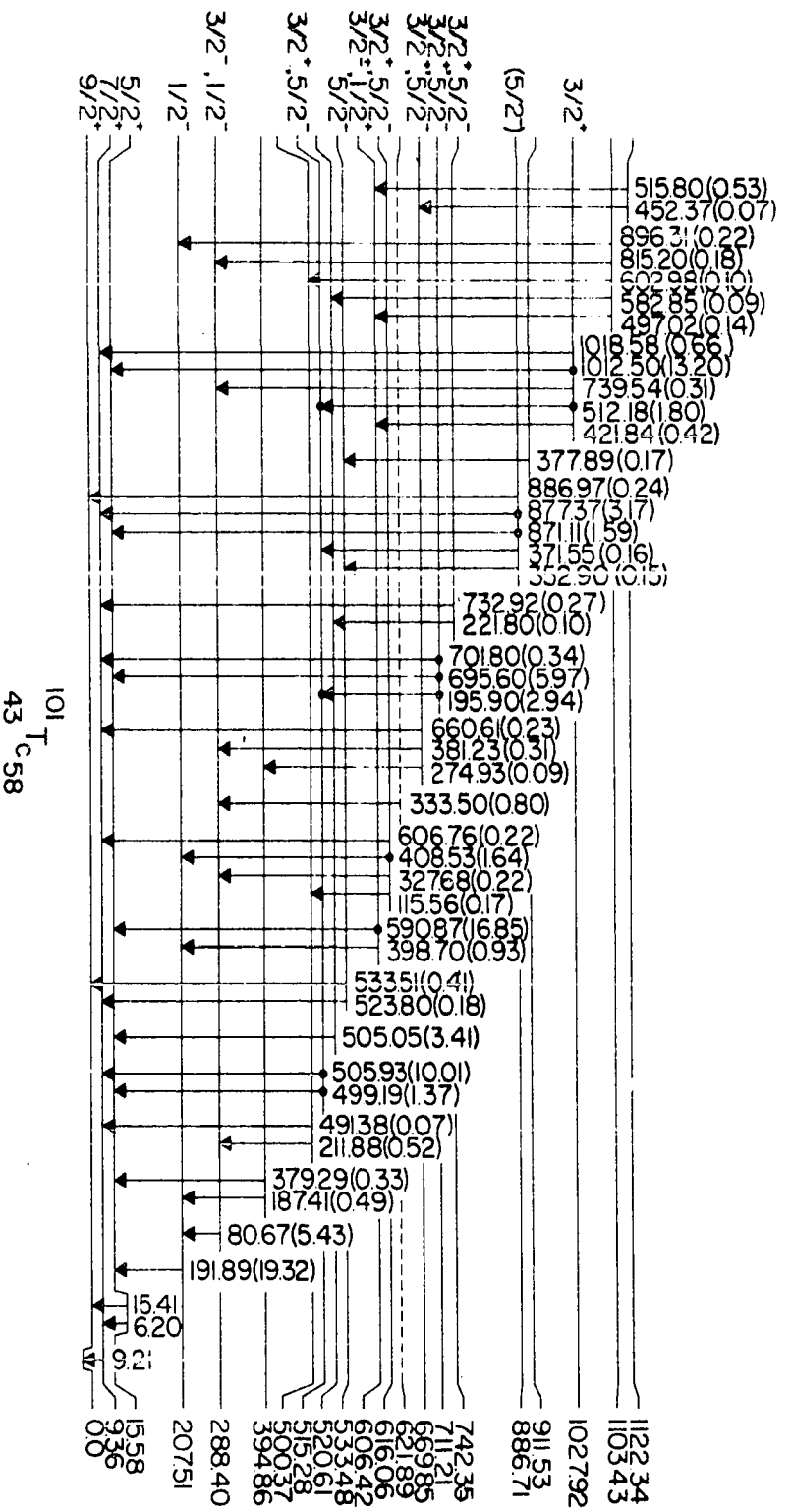

Figure 8. The ^{101}Tc level scheme

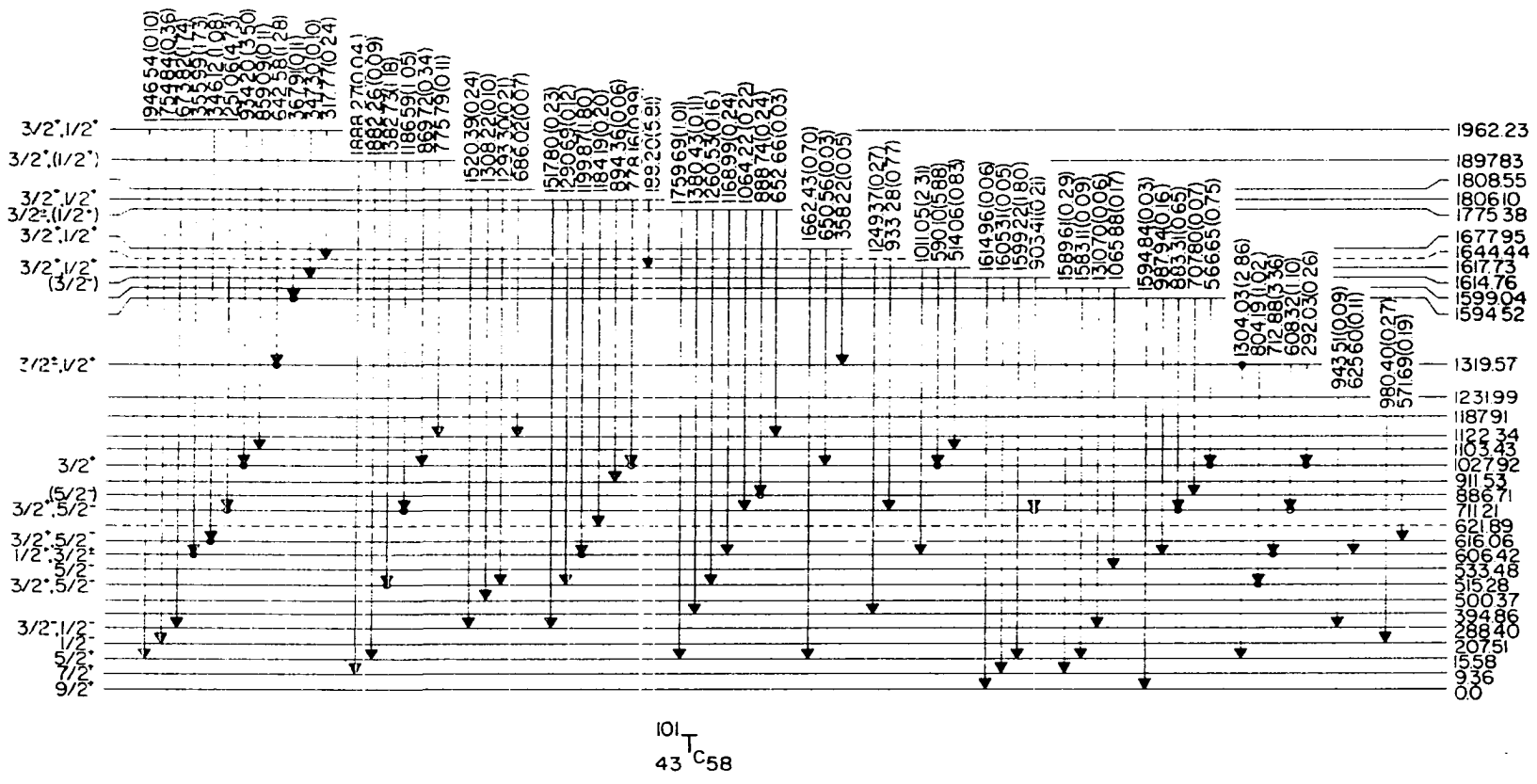

Figure 8. (continued)

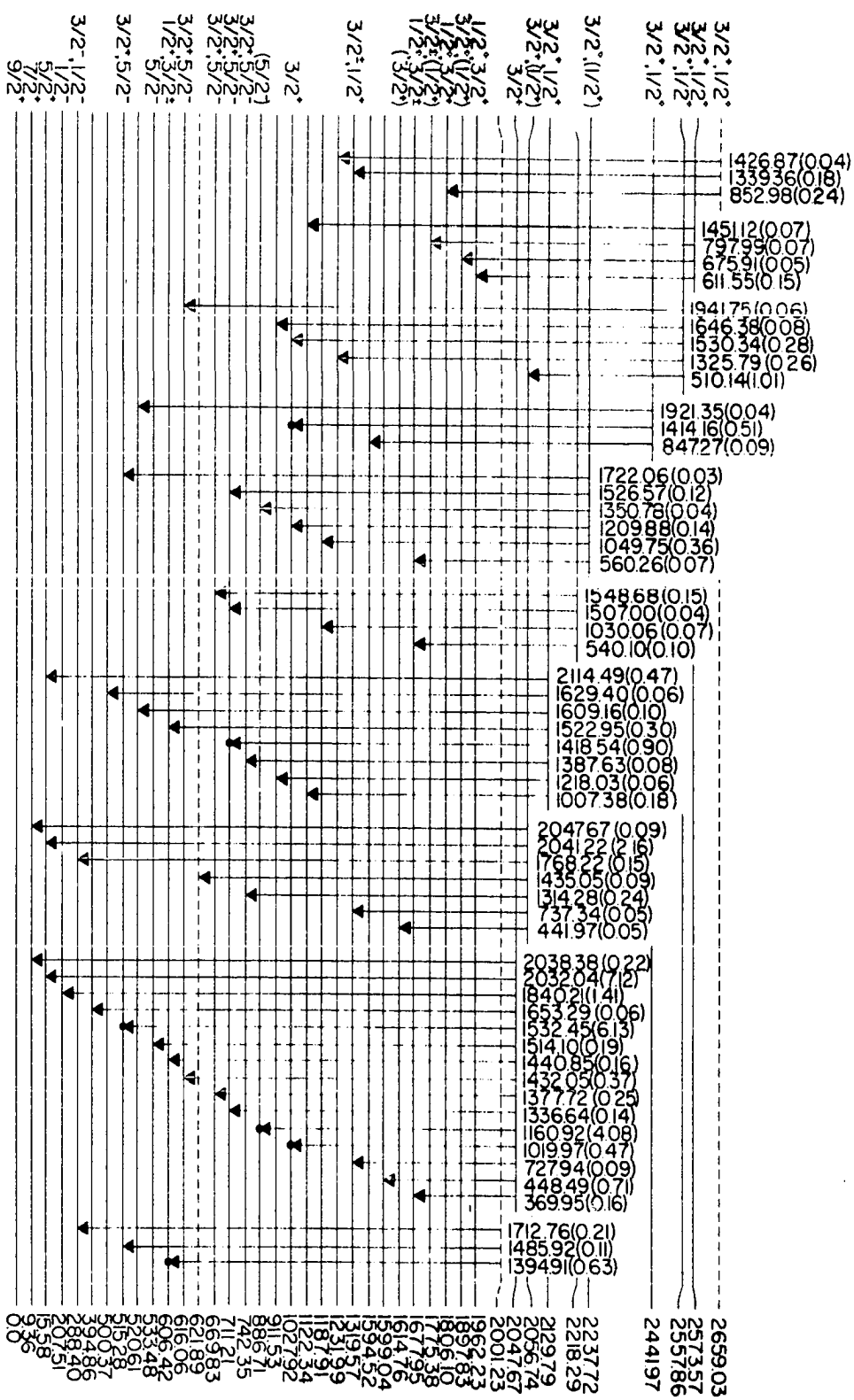

Figure 3. (continued)

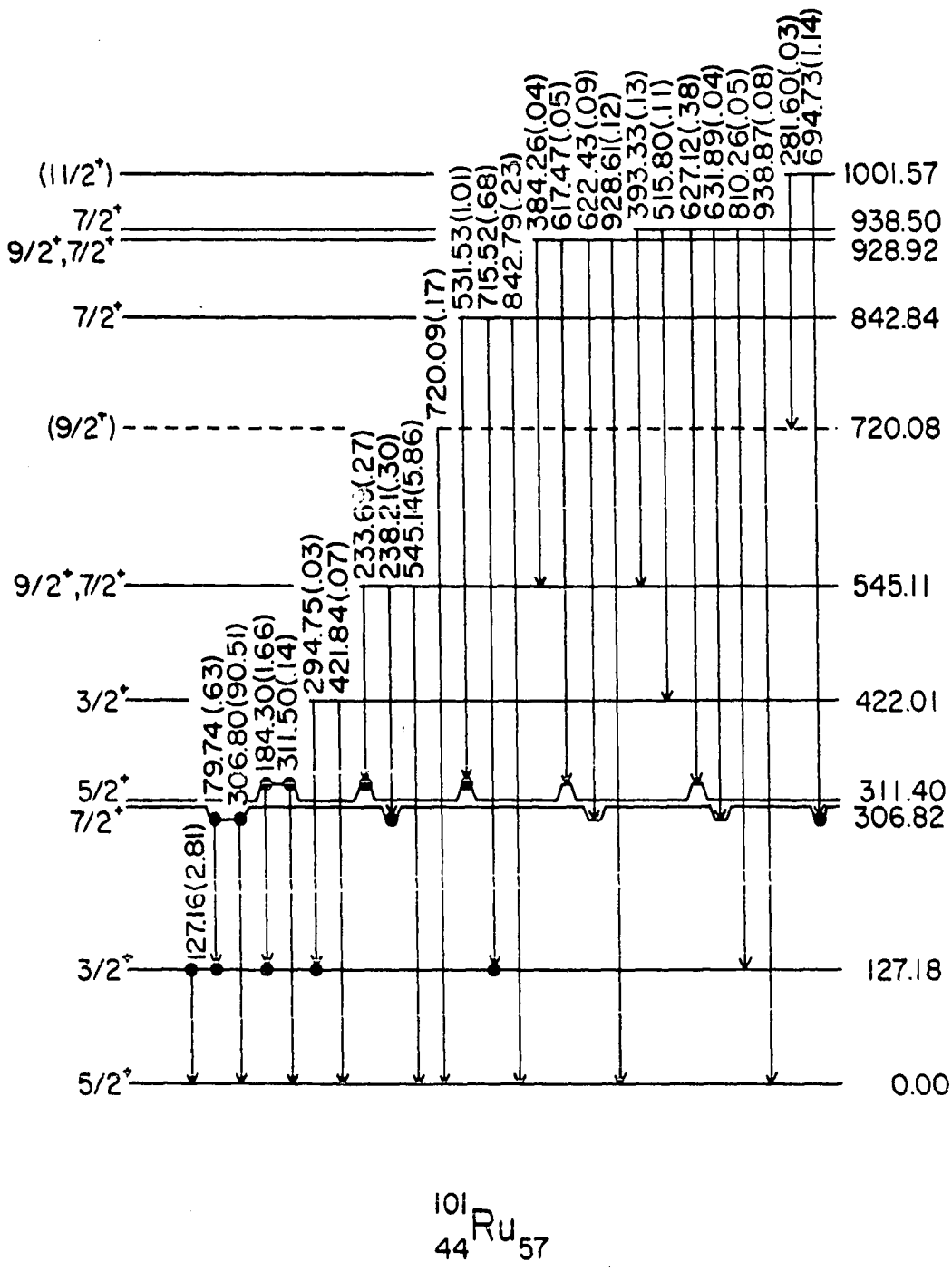

Figure 9. The ^{101}Ru level scheme

schemes shown in Figures 8 and 9. The levels indicated by a solid line are judged to be firm levels. In Figures 8 and 9 the intensities are given as gamma rays/100 decays and the energies are in keV.

The Q-value of the Tc beta decay has been reported to be 1.32 MeV, as found by analysis of the beta spectrum in coincidence with the intense 307-keV gamma ray (19). The decay energy for Mo is reported to be 2.23 ± 0.04 MeV (20). In this work, gamma-ray intensity imbalances were used to get the beta feedings of the excited levels. The percent beta feedings to a particular level were determined by assuming no beta decay to the ground state of either ^{101}Tc or ^{101}Ru. The log ft values were calculated using LOGFT (Appendix A) and the results are summarized in Tables 7 and 8.

E. Conclusions

Several rules were followed in determining the spins (J) and parities (π) for the levels given in Figures 8 and 9. The standard rules on these assignments based on log ft values were suggested by Raman and Gove (21), and are listed below.

log ft ≤ 5.9	$\Delta J = 0,1$	$\Delta\pi$ = no
log ft ≤ 8.5	$\Delta J = 0,1$	$\Delta\pi$ = yes or no
log ft < 11	$\Delta J = 0,1$	$\Delta\pi$ = yes or no
	or $\Delta J = 2$	$\Delta\pi$ = yes
log ft < 12.8	$\Delta J = 0,1,2$	$\Delta\pi$ = yes or no

Table 7. Summary for beta fed levels in ^{101}Tc

Level Energy (keV)	Percent Beta Feeding	Log ft
207.51(.12)	10.46(1.4)	6.92(.06)
288.40(.10)	3.63(.66)	7.32(.08)
394.86(.17)	0.29(.18)	8.35(.28)
500.37(.14)	0.10(.09)	8.74(.39)
515.28(.16)	<1.76	>7.47
520.61(.14)	0.92(.48)	7.51(.23)
533.48(.20)	<0.03	>9.16
606.42(.21)	5.81(2.9)	6.88(.22)
616.06(.13)	0.62(.17)	7.84(.12)
621.89(.11)	0.50(.06)	7.93(.05)
669.83(.16)	0.16(.06)	8.40(.17)
711.21(.06)	<0.66	>7.74
742.35(.14)	<0.14	>8.39
886.71(.13)	0.86(.40)	7.47(.20)
911.53(.26)	<0.07	>8.51
1027.92(.17)	3.17(2.9)	6.77(.40)
1122.34(.15)	0.15(.14)	8.02(.41)
1187.91(.11)	<0.08	>8.22
1231.99(.20)	<0.01	>8.98
1319.57(.11)	6.81(.29)	6.14(.03)
1594.52(.09)	1.43(.25)	6.48(.08)
1614.76(.11)	1.92(.10)	6.33(.04)
1617.73(.26)	<6.38	>5.80
1644.44(.14)	0.79(.47)	6.67(.26)
1677.95(.19)	0.44(.12)	6.88(.12)
1775.38(.17)	1.88(.11)	6.10(.04)
1806.10(.10)	9.28(2.5)	5.36(.12)
1808.55(.18)	0.61(.06)	6.54(.05)
1897.83(.11)	2.72(.15)	5.75(.04)
1962.23(.10)	14.62(.61)	4.90(.04)
2001.23(.13)	0.92(.06)	6.03(.05)
2047.67(.16)	20.23(.59)	4.60(.04)
2056.74(.11)	2.68(.13)	5.46(.04)
2129.79(.16)	2.09(.09)	5.41(.05)
2218.29(.25)	0.36(.07)	5.98(.10)
2237.72(.18)	0.74(.05)	5.61(.06)
2441.97(.15)	0.63(.04)	5.07(.08)
2557.86(.15)	1.66(.17)	4.16(.11)
2573.57(.23)	0.33(.07)	4.78(.14)
2659.03(.12)	0.45(.03)	4.11(.16)

Table 8. Summary for beta fed levels in ^{101}Ru

Level Energy (keV)	Percent Beta Feeding	Log ft
127.17(.13)	<.35	>7.41
306.82(.07)	89.28(7.0)	4.79(.04)
311.38(.07)	0.19(.15)	7.44(.34)
422.07(.37)	<.04	>7.98
545.10(.06)	6.17(.44)	5.62(.04)
720.08(.23)	0.14(.03)	6.99(.11)
842.83(.08)	1.88(.12)	5.62(.04)
928.92(.30)	0.30(.04)	6.24(.06)
938.50(.27)	0.79(.07)	5.80(.05)
1001.57(.27)	1.15(.69)	5.49(.26)

Since, in many cases, spin-parity ambiguities can result from beta decay branches, it is useful to consider the gamma rays leaving or populating a level in an attempt to further limit the spin-parity possibilities. The rules governing gamma-ray transitions are best summarized by considering the parity change of the transition. If a parity change is made, a transition will be most probably E1, but could possibly be M2 in competition with E1 for very weak transitions. If the parity is unchanged, E2 or M1 transitions should prevail. In the case of isomeric transitions, however, higher order multipolarities are observed. In the assignments made in this work, use was made of gamma-ray transitions for limiting spin-parity assignments, as discussed separately for each level scheme.

The nuclear levels of ^{101}Ru have been studied recently by several groups(9-11), and their results are in general agreement with those of this work. The only other ^{101}Tc decay study leading to levels in ^{101} Ru which used Ge(Li)-Ge(Li) coincidence techniques was by Cook and Johns(11). Several differences exist between this work and that of Cook and Johns, as detailed below.

Cook and Johns report a 616.2-keV level which is not populated by gamma rays and has only a single depopulating gamma ray of 489-keV, in coincidence with the 127-keV

transition. This level is seen in Coulomb excitation studies (22) and in the decay of ^{101}Rh (23). In this work, of comparable sensitivity to that of Cook and Johns, the 489-keV gamma ray was not seen in either singles or coincidence spectra and there was no other evidence to indicate a level at 616-keV. Accordingly, the 616-keV level is not included in this work.

The 720.08-keV level that is dashed in this work is reported as a firm level by Cook and Johns (11). The CI of this level (2) was insufficient to warrant assignment as a firm level.

The 1001.57-keV level is substantiated by the presence of the 360.8-keV gamma ray in the 694-keV coincidence gate. This level is not reported by Cook and Johns (11) but is seen in the ^{100}Mo(α,3n)^{101}Ru studies by Lederer, Jaklevic and Hollander (24).

No single known nuclear model can adequately describe the ^{101}Ru nucleus. The ground state spin has been measured as J=5/2 (25). This is consistent with a ground state neutron configuration of $(g_{7/2})^6(d_{5/2})^1$ (see Figures 3 and 18). The 306.82-keV state probably has the $(g_{7/2})^5(d_{5/2})^2$ configuration, as indicated by the strong beta group feeding this level. This beta decay probably involves the "allowed" beta transition of a $g_{9/2}$ proton to a $g_{7/2}$ neutron.

The energy of the first excited 2+ state of ^{100}Ru is at 450-keV (26). The coupling of a $d_{5/2}$ neutron to this state should give a series of levels with J of 1/2+, 3/2+, 5/2+, 7/2+ and 9/2+, with a center of gravity at 450 keV, according to a simple particle-core coupling scheme. The 127.18(3/2+), 311.40(5/2+) and 842.84(7/2+) levels are possible choices because of their decay properties. However, no 9/2+ state appears to decay predominantly to other members of this coupling multiplet. The 842-keV level is depopulated principally to the 311-keV and 127-keV states. The 311-keV level is depopulated more strongly to the 127-keV level than to the ground state. No 1/2+ state is apparent in this work, which is not surprising, considering the high parent activity spin of 1/2+. These attempts to fit a particle-plus-core coupling model to ^{101}Ru is considered to be speculative, especially in view of the lack of information on transition multipolarities and level characteristics from stripping or pick-up reaction studies.

The ^{101}Tc levels are more numerous than the ^{101}Ru levels. The spins and parities of the levels were determined using the rules mentioned above, along with some other basic restrictions. If the choice could not be narrowed to three or less spins and parities for a particular level, no assignment was made. Observed gamma-ray transitions were assumed to have only E1, M1 or

E2 multipolarities, and the presence of transitions to the 7/2+ level at 9 keV was instrumental in discarding some possible spin assignments.

The following levels are postulated in this work but not indicated by Cook and Johns (11): 520.61, 911.53, 1122.34, 1617.73, 1644.44, 1808.55, 2218.29, 2441.97, 2557.86, 2573.57 and 2659.03 keV. The 1617-keV state has four gamma rays associated with other firm levels. One of these gamma rays, at 590.1 keV, was found to be coincident with the 1012.5-keV gamma ray which depopulates the 1027.92-keV level. The 2441.97-keV level is connected with three firm levels. The 1414.16-keV gamma ray is coincident with the 512.18-keV gamma ray. These two gamma rays are in a cascade involving the 2441.97-, 1027.97-, and 515.28-keV states.

The 911.53-, 1808.55-, 2218.29- and 2573.57-keV states are all connected with sets of four known levels. The 2557.86-keV state is connected to five firm levels by gamma transitions and the 1122.34-keV state is connected to seven firm levels by gamma transitions. The level at 520.61 keV is associated with five other states, four of which are firm levels. The 1644.44- and 2659.03-keV levels are only associated with three other levels and are dashed to indicate a lack of firmness.

Cook and Johns report the 1025.59-, 1141.5-, 1197.3-, 1449.0-, 1565.09-, 1829.9-, 1928.88-, 2150.3-, and 2252.6-keV levels that were not deduced in this work The 2252.6-keV level is associated with only one gamma ray, with this gamma ray found in the coincidence spectra. In this work, the gamma ray was seen in the singles spectrum but not in the coincidence spectra. The 1197.3- and 1892.9-keV levels are also just associated with a single gamma ray per level, listed as a possible coincidence. Neither of the gamma rays were seen in this work. The 1025.59- and 2150.3-keV states are connected to other levels by two gamma rays apiece, with one of each being a coincident gamma ray. Both the coincident gamma ray for the 1025-keV level and the gamma ray, not verified by coincidences, for the 2150-keV level were seen in this work in the equilibrium singles experiment. The 1141.5-keV level is connected to two levels by possible coincidences, one of which is seen in this work in the singles spectrum The 1449.0- and 1565.09-keV states are the middle states of gamma-ray cascades, the cascades being listed in the coincidence data of Cook and Johns. Neither of the gamma rays associated with the 1449-keV level and only one of the gamma rays associated with the 1565-keV state were seen in this work's singles spectrum. The 1928.88-keV level has four gamma rays associated with it, with three of them found in the coincidence spectra. These

four gamma rays were not seen in the singles or coincidence spectra of this work.

It might also be mentioned that Cook and Johns have placed 139 gamma rays in 45 levels for an average of 3.089 gamma rays per level. This work has placed 169 gamma rays in 45 levels for an average of 3.756 gamma rays per level. Their singles experiments were performed using a 12 cm^3 Ge(Li) detector with a resolution of 2.9 keV at 1332 keV and a thin window Ge(Li) detector with a resolution of 700 eV at 122 keV. Their coincidence data was collected with 36-cm^3 and 40-cm^3 Ge(Li) detectors.

The reader is referred to Part I of this work for a discussion of a five-particle shell-model calculation as applied to ^{101}Tc.

III. NUCLEAR DECAYS OF ^{142}Xe AND ^{142}Cs

A. Introduction

Previous work on the short-lived activities ^{142}Xe and ^{142}Cs has been done at the Ames Laboratory by Larsen, Talbert and McConnell (27) and by Adams *et al.* (28). Adams *et al.* determined the beta decay energy of the ^{142}Xe decay to be 4.9 ± 0.1 MeV and the beta decay energy for ^{142}Cs decay to be 6.89± 0.06 MeV. The work by Larsen *et al.* reported preliminary level schemes for ^{142}Cs and ^{142}Ba. The half-lives for the ^{142}Xe and ^{142}Cs decays have been measured to be 1.24 and 1.68 sec, respectively (29).

The motivation for this work came from the need to extend the previous experimental results to obtain a better knowledge of nuclear systematics in this region.

B. Experimental Procedure

A sample of fully enriched ^{235}U in the stearate form is placed in a neutron beam of 3 X 10^9 neutrons/cm^2-sec at the Ames Laboratory Research Reactor. The sample is spread out on several shallow trays in an aluminum container. As the sample undergoes fission, the noble gas products emanate and drift to the ion source of the isotope separator through a 1.6-m transport line. A sweep gas, composed of 1% stable Kr, 1% stable Xe and 98% stable He, is used to decrease the transport time to the ion source.

1. TRISTAN

A schematic view of the TRISTAN on-line isotope separator (30) is shown in Figure 10. The ion source ionizes the fission products and the sweep gas. Differential pumping removes the un-ionized molecules as the ions are extracted, then accelerated through 50 kV. The ion beam is then focused by a pair of electrostatic lenses and introduced into a 1.6-m, 90° analyzing magnet. The mass of interest is selected from the fully dispersed ion beam in the collector box, at the magnet focal plane, by means of a slit that allows only the mass of interest to proceed to the switching magnet. The switching magnet further focuses and purifies the beam while directing it to one of the experimental facilities.

2. Isobaric separation

The mass distribution of fission products from ^{235}U is shown in Figure 11. Only the ^{142}Xe member of the A=142 isobaric chain is emanated in a sufficient quantity to be studied at the experimental ports of TRISTAN. The ion beam is deposited at the moving tape collector (MTC), which contains about 610 m of 0.025-mm thick aluminized mylar. The MTC has two ports at the point of beam deposit and two additional ports at a location shielded from the point of deposit by lead bricks. Isobaric separation of the members

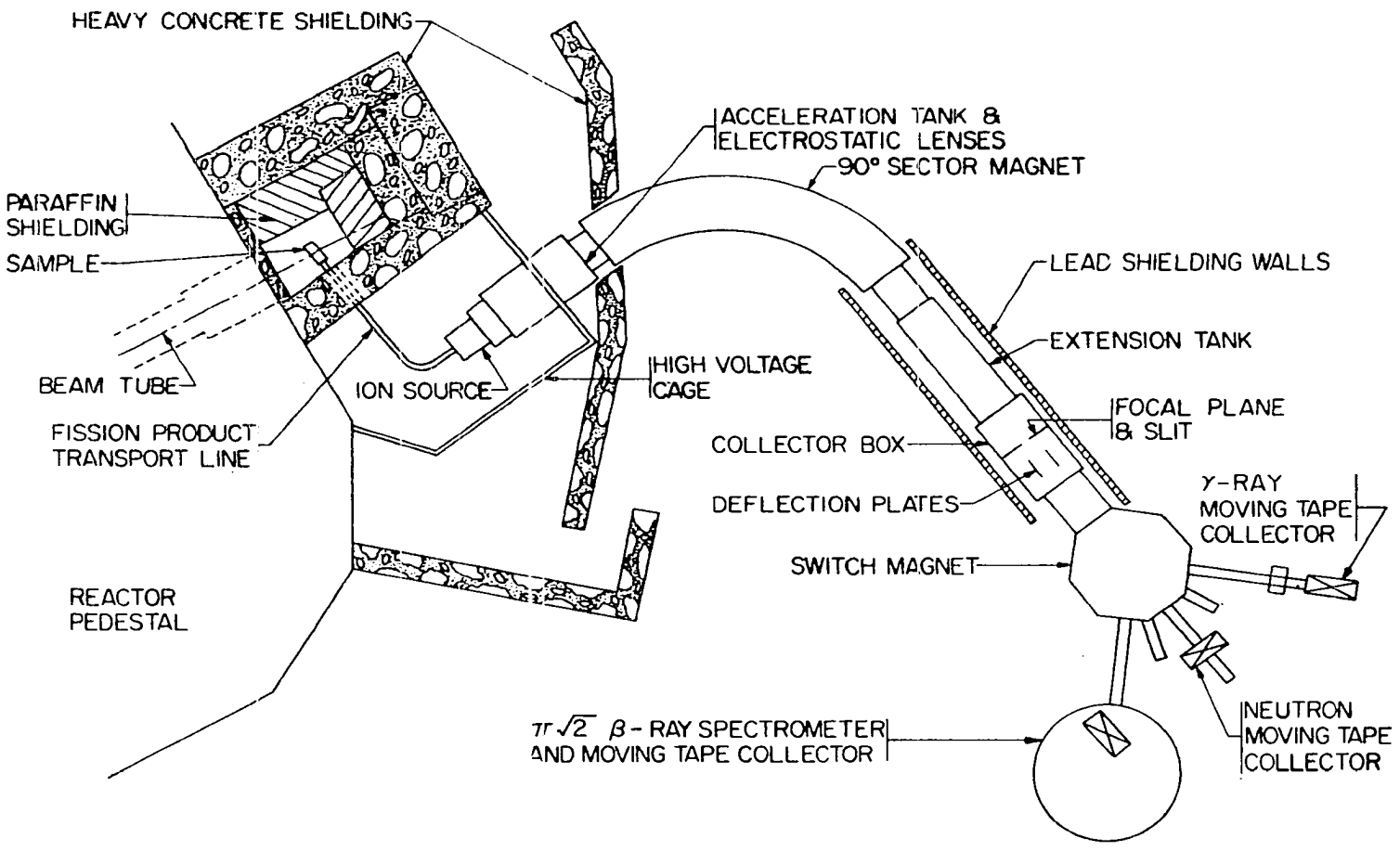

Figure 10. A schematic view of the TRISTAN on-line isotope separator facility

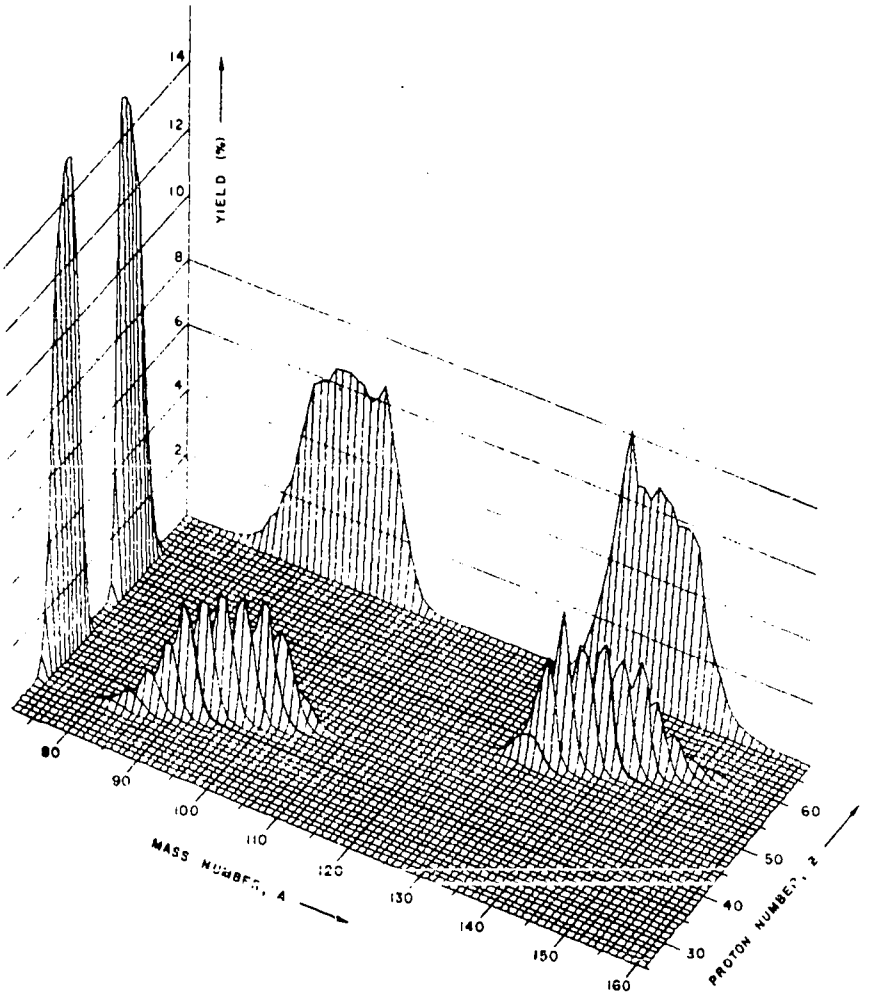

Figure 11. ^{235}U fission product yield distribution

of a decay chain can be accomplished by use of the MTC in one of three modes. The parent activity can be optimized by continuously moving the tape and therefore removing the daughter from the ports at the point of deposit. To study a short-lived daughter, the MTC can be used with collect, delay, accumulate and transport times operated sequentially. In other words the beam is deposited, the parent decays, the short-lived daughter is counted and then the longer-lived daughters are removed from the detector ports. The last method of operation is used when a longer-lived daughter is to be studied. The MTC is used with collect-transport and delay-accumulate times operated sequentially. In other words, the beam is deposited at the first port, then moved to the second set of ports where the detectors are located. The short-lived activity is allowed to die off, then the longer-lived activity is counted. Times used to optimize the activity of a particular sample are determined by the program ISOBAR described in Reference 31.

The ^{142}Xe-^{142}Cs activity was collected for 30-min periods at the beam deposit port of the MTC. After this time interval, the tape was moved to eliminate continued buildup of the long-lived daughter activites ^{142}Ba, $T_{1/2}$ = 10.7 min, and ^{142}La, $T_{1/2}$ = 92 min (29). The detectors used in the experiment are listed in Appendix B. Block diagrams

and general descriptions of the experimental systems are also given in Appendix B. The gamma-ray spectrum of the ^{142}Xe-^{142}Cs decay is shown in Figure 12. It should be noted that the spectrum from 15 to 270 keV was obtained using the 1-cc LEPS detector while the 57.3-cc Ge(Li) detector was used for the other five spectra of Figure 12.

C. Data Analysis

The singles and coincidence spectra were analyzed using the programs SKEWGAUS and DRUDGE in the same manner that the A=101 data was analyzed. The assignment of photopeaks to either the Xe or Cs decay was made from the assignments reported by Larsen *et al.* derived from comparison of an equilibrium spectrum to a spectrum that had been enhanced in Xe decay by the MTC daughter analysis unit.

The gamma-ray calibration sources given in Appendix B are inadequate for energies greater than about 3500 keV. When the pair production interaction is likely in a Ge(Li) detector, additional spectrum peaks are seen at the gamma-ray energies minus 1022 and 511 keV. These peaks are called double- and single-escape peaks, respectively. A precise energy calibration above 3500 keV was determined by using double-escape peaks to locate exact energies of the parent peaks.

The gamma-ray lists for the ^{142}Xe and ^{142}Cs decay are given in Tables 9 and 10, respectively. The results of the

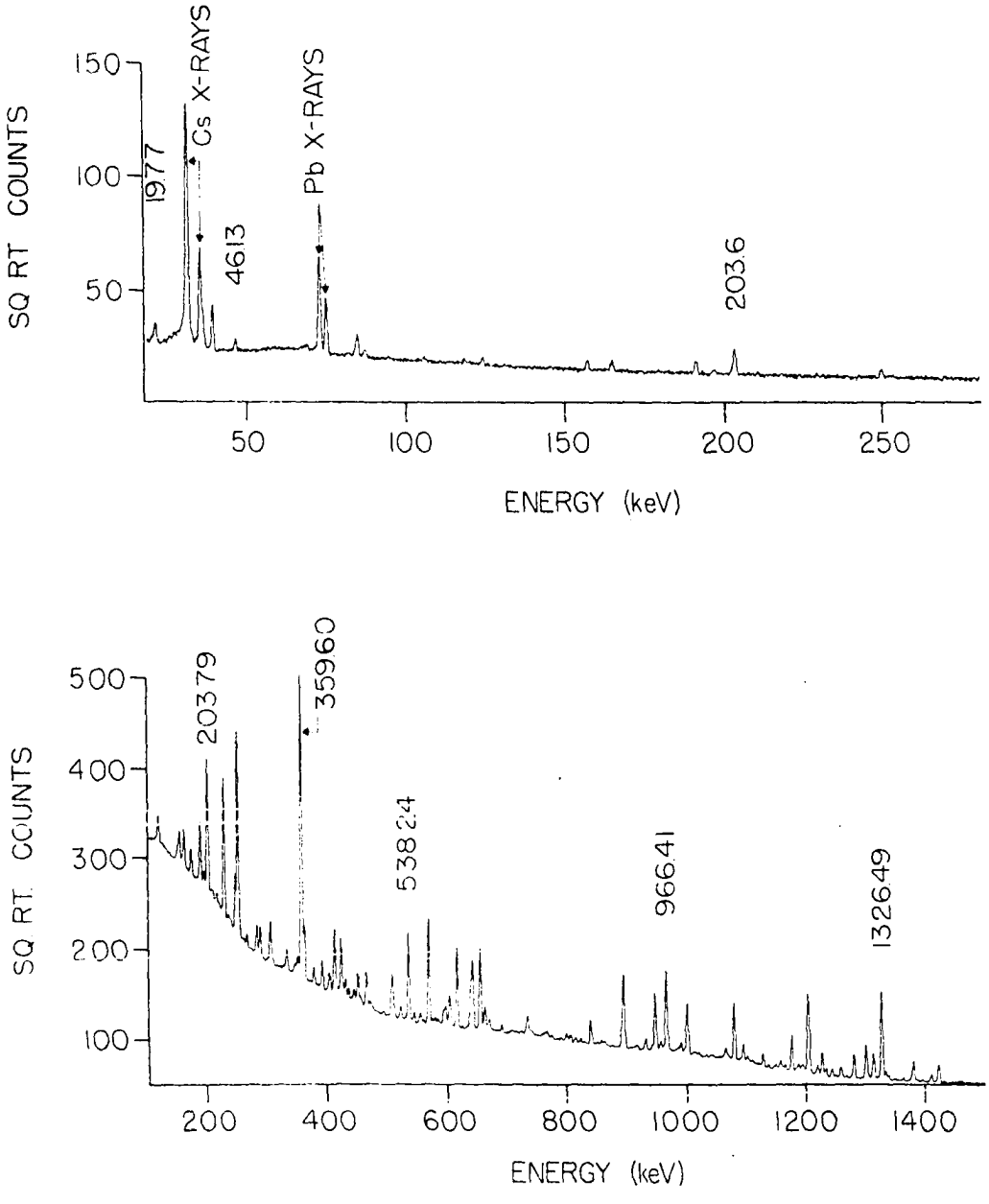

Figure 12. The gamma-ray spectrum for the equilibrium decay of ^{142}Xe and ^{142}Cs

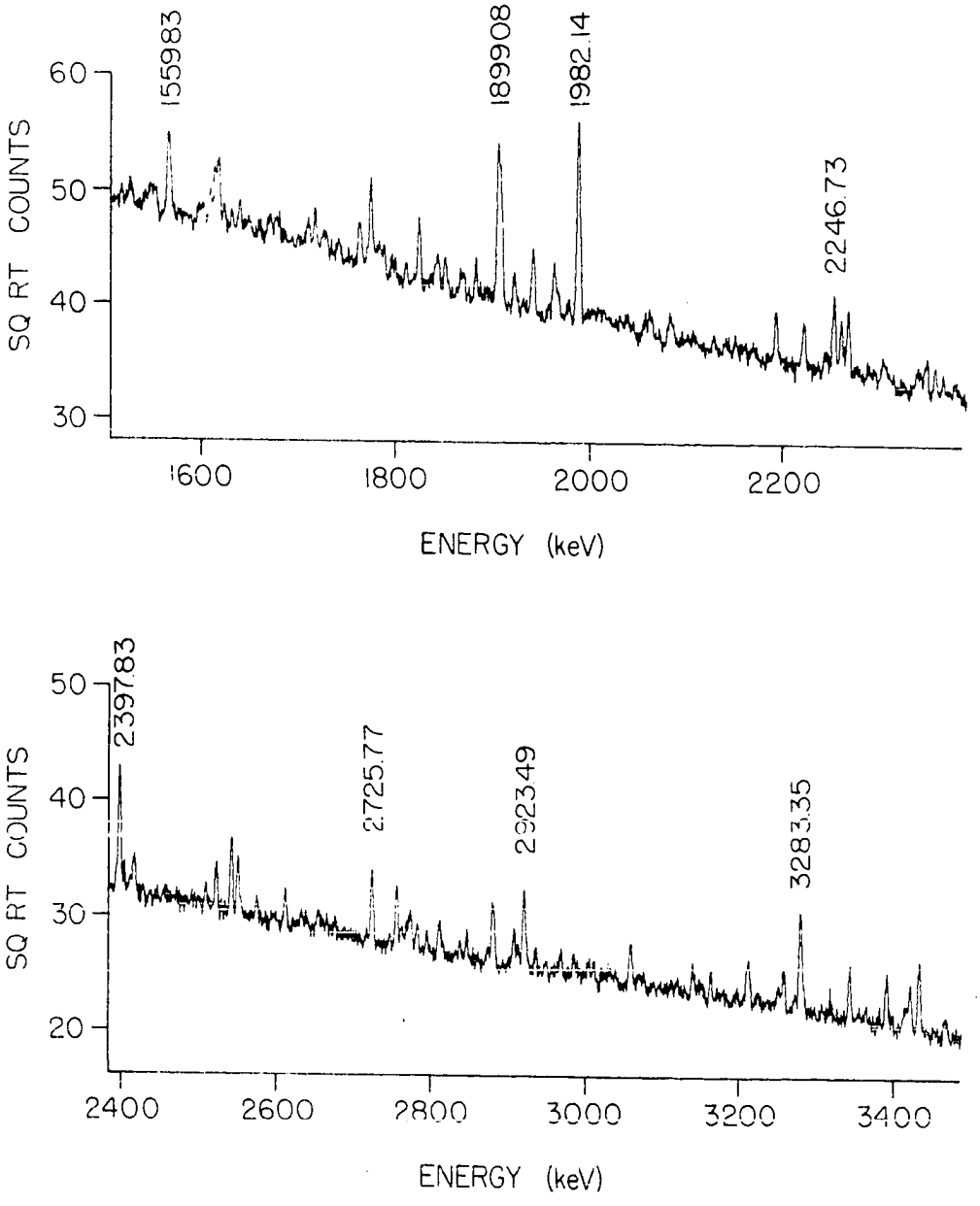

Figure 12. (continued)

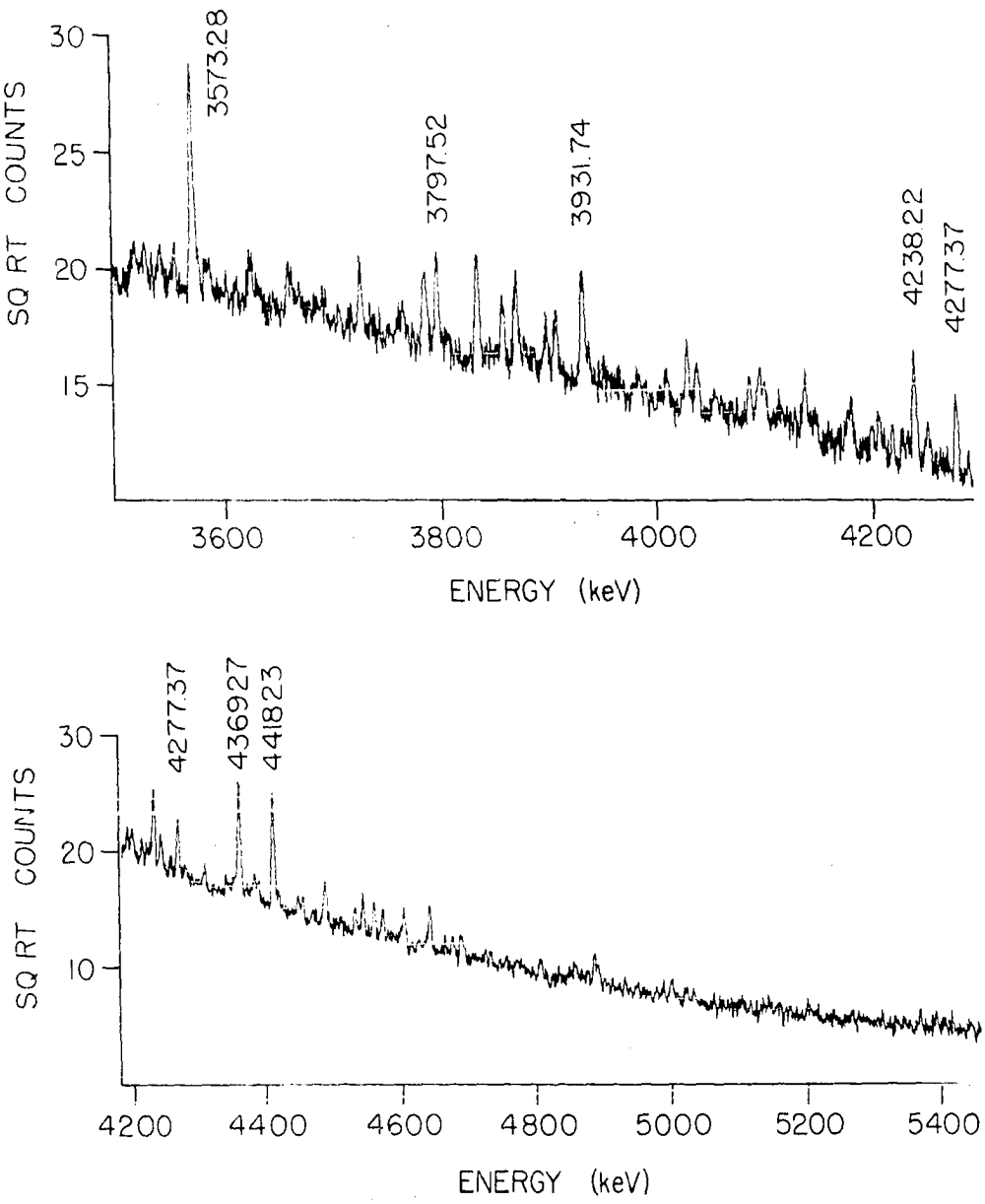

Figure 12. (continued)

Table 9. Gamma-ray transitions in ^{142}Cs

Energy (keV)	Relative[1] Intensity	Assignment
12.20 *	1.54	12. -> 0.
19.77(0.13)	32.30(9.07)	776. -> 757.
20.80(0.08)	134.59(11.38)	
33.00 *	0.32	243. -> 210.
38.83(0.07)	22.01(3.01)	39. -> 0.
38.83(0.07)	233.36(17.27)	243. -> 204.
46.13(0.09)	49.50(8.02)	85. -> 39.
57.50 *	0.14	657. -> 600.
57.50 *	0.14	70. -> 12.
70.10(0.40)	23.70(10.16)	70. -> 0.
72.86(0.06)	274.26(16.52)	85. -> 12.
94.61(0.26)	15.03(9.24)	304. -> 210.
100.80(0.57)	3.69(1.19)	757. -> 657.
100.80(0.57)	3.69(1.19)	304. -> 204.
105.61(0.24)	19.77(2.78)	1195. -> 1090.
113.36(0.25)	17.78(2.71)	
117.53(0.32)	22.86(4.44)	
119.87(0.36)	25.39(4.13)	776. -> 657.
124.52(0.18)	85.53(17.78)	210. -> 85.
157.55(0.09)	174.17(10.97)	243. -> 85.
161.70(0.23)	32.84(4.23)	
165.06(0.09)	217.75(12.60)	204. -> 39.
167.42(0.61)	17.47(6.06)	944. -> 776.
170.98(0.43)	15.17(3.69)	210. -> 39.
191.70(0.08)	356.71(20.01)	204. -> 12.
197.44(0.14)	67.72(8.43)	210. -> 12.
203.79(0.07)	275.68(14.22)	204. -> 0.
203.79(0.07)	644.95(29.12)	243. -> 39.
211.66(0.34)	38.67(8.77)	251. -> 39.
219.11(0.27)	53.73(10.19)	304. -> 85.
239.52(0.39)	39.85(11.65)	
242.83(0.58)	26.99(12.60)	243. -> 0.
250.68(0.09)	320.14(21.70)	251. -> 0.
264.25(0.27)	15.64(3.49)	304. -> 39.
286.66(0.07)	170.92(9.31)	943. -> 657.

[1]Relative to 571.83 keV transition
*Gamma ray too weak to be seen at this energy

Table 9. continued)

Energy (keV)	Relative[1] Intensity	Assignment
291.95(0.07)	175.39(9.41)	304. -> 12.
304.30(0.36)	17.44(5.25)	304. -> 0.
309.06(0.07)	272.09(14.76)	
312.99(0.23)	30.68(5.42)	732. -> 419.
330.22(0.22)	22.86(2.91)	
334.73(0.10)	122.98(8.16)	
337.06(0.46)	20.59(5.01)	
349.04(0.30)	57.83(11.51)	600. -> 251.
352.97(0.15)	126.63(13.44)	657. -> 304.
373.42(0.47)	8.97(3.56)	
379.90(0.08)	102.97(6.23)	419. -> 39.
394.20(0.10)	174.54(11.34)	598. -> 204.
404.45(0.44)	20.04(4.91)	2500. -> 2095.
406.47(0.10)	109.60(7.79)	657. -> 251.
414.52(0.07)	467.97(24.58)	657. -> 243.
418.47(0.31)	35.92(5.82)	419. -> 0.
421.77(1.07)	11.95(5.89)	
428.44(0.23)	54.89(6.43)	732. -> 304.
432.36(0.16)	115.76(11.38)	1090. -> 657.
438.19(0.17)	62.88(6.40)	1195. -> 757.
447.23(0.11)	69.78(6.77)	657. -> 210.
453.15(0.07)	198.89(11.55)	657. -> 204.
468.17(0.07)	202.48(12.19)	719. -> 251.
468.17(0.07)	33.86(2.03)	1068. -> 600.
497.46(0.26)	22.86(4.57)	
524.44(0.11)	75.74(6.03)	1614. -> 1090.
538.24(0.07)	768.57(40.80)	1195. -> 657.
547.69(0.21)	67.35(11.24)	757. -> 210.
557.82(0.19)	74.46(8.94)	
562.19(0.39)	25.26(6.81)	
571.83(0.06)	1000.00(51.53)	657. -> 85.
577.92(0.30)	33.83(6.70)	
582.49(0.24)	43.71(7.14)	886. -> 304.
587.10(0.35)	29.56(7.38)	657. -> 70.
605.56(0.08)	220.05(13.51)	
618.06(0.07)	720.97(40.63)	657. -> 39.
627.41(1.94)	8.46(11.00)	
644.80(0.07)	632.90(35.08)	657. -> 12.
657.05(0.06)	791.02(40.50)	657. -> 0.
661.91(0.47)	29.73(7.55)	732. -> 70.

Table 9. continued)

Energy (keV)	Relative[1] Intensity	Assignment
664.58(0.11)	168.38(11.58)	
669.07(0.42)	28.10(5.93)	
672.20(0.19)	73.85(7.08)	757. -> 85.
693.60(0.10)	51.67(3.83)	732. -> 39.
709.05(0.30)	19.54(4.40)	
718.20(0.39)	7.08(2.37)	757. -> 39.
718.20(0.39)	7.08(2.37)	719. -> 0.
724.34(0.65)	12.60(5.69)	
727.08(0.42)	18.49(5.82)	978. -> 251.
735.45(0.35)	64.23(14.25)	
737.37(0.17)	126.02(16.32)	776. -> 39.
741.03(0.26)	33.22(4.47)	
744.36(0.24)	30.54(4.40)	757. -> 12.
761.65(0.35)	17.71(3.69)	
765.66(0.21)	33.93(4.03)	1195. -> 1961.
776.05(0.20)	27.53(3.89)	776. -> 0.
792.18(0.28)	22.96(4.67)	
801.24(0.19)	62.00(6.94)	886. -> 85.
807.39(0.26)	56.85(8.43)	1876. -> 1068.
815.88(0.21)	36.30(5.52)	886. -> 70.
823.52(0.19)	34.40(4.00)	
829.65(0.35)	12.53(3.32)	
862.90(0.21)	27.22(4.33)	1067. -> 204.
891.40(0.13)	112.04(9.11)	1195. -> 304.
917.64(0.31)	29.73(5.62)	1984. -> 1067.
930.26(0.31)	23.50(4.60)	
943.79(0.48)	28.54(9.92)	943. -> 0.
957.27(0.21)	66.87(9.65)	1614. -> 657.
983.48(0.48)	24.82(6.23)	1068. -> 85.
991.23(0.11)	88.10(6.84)	1195. -> 204.
996.41(0.21)	36.40(5.08)	1067. -> 70.
1020.15(0.27)	25.97(4.60)	
1040.36(0.48)	15.54(4.13)	1984. -> 944.
1068.29(0.27)	26.48(4.81)	1068. -> 0.
1089.71(0.52)	12.46(4.10)	1090. -> 0.
1108.33(0.31)	7.11(0.27)	1312. -> 204.
1156.80(0.14)	66.26(4.98)	1876. -> 718.
1164.72(0.22)	30.47(3.59)	
1183.45(0.36)	27.36(4.94)	1195. -> 12.

Table 9. continued)

Energy (keV)	Relative[1] Intensity	Assignment
1187.39(0.18)	57.56(5.76)	2500. -> 1312.
1195.43(0.30)	45.03(7.04)	1195. -> 0.
1219.23(0.22)	62.20(8.46)	1876. -> 657.
1227.01(0.07)	188.90(10.77)	1312. -> 85.
1232.99(0.16)	48.28(4.84)	
1257.96(0.11)	77.20(5.93)	
1300.09(0.06)	305.78(16.15)	1312. -> 12.
1303.97(0.31)	24.21(4.06)	1961. -> 657.
1312.29(0.06)	213.62(11.72)	1312. -> 0.
1338.28(0.33)	28.75(5.72)	2095. -> 757.
1363.32(0.31)	17.88(3.39)	1961. -> 598.
1376.58(0.30)	22.08(3.01)	2095. -> 719.
1384.47(0.41)	16.86(2.95)	1984. -> 600.
1395.04(0.27)	17.27(2.51)	2282. -> 886.
1410.60(0.10)	58.95(4.30)	1614. -> 204.
1431.67(0.55)	12.29(3.86)	2500. -> 1068.
1456.50(0.55)	12.32(3.83)	1876. -> 419.
1486.94(0.98)	6.50(3.72)	
1511.70(0.78)	6.67(2.98)	
1520.41(0.46)	11.48(3.18)	
1595.12(0.45)	13.88(3.66)	
1602.15(0.32)	19.40(3.59)	1614. -> 12.
1607.01(0.22)	34.94(4.00)	
1616.33(0.57)	10.23(3.22)	
1624.76(0.74)	7.75(3.25)	1876. -> 251.
1632.90(0.40)	14.42(3.45)	1876. -> 243.
1710.88(0.27)	21.23(3.42)	1961. -> 251.
1718.87(0.82)	9.31(3.89)	1961. -> 242.
1773.28(0.67)	12.73(4.71)	
1781.67(0.43)	17.37(5.76)	2500. -> 719.
1789.51(0.76)	10.53(4.13)	1876. -> 85.
1804.63(0.51)	11.58(3.35)	1876. -> 70.
1837.13(0.48)	18.59(4.47)	1876. -> 39.
1844.51(0.32)	20.25(3.69)	2095. -> 251.
1862.19(0.58)	14.80(4.64)	2282. -> 419.
1875.76(0.50)	17.27(4.88)	1876. -> 0.
1902.05(0.18)	75.57(7.04)	2500. -> 598.
1972.13(1.49)	5.79(4.74)	1984. -> 12.
2077.66(0.53)	16.49(4.54)	2282. -> 204.

Table 10. Gamma-ray transitions in ^{142}Ba

Energy (keV)	Relative[1] Intensity	Assignment
100.60(0.50)	0.00(0.00)	
209.32(0.74)	5.12(2.51)	1536. -> 1327.
325.00(0.50)	2.63(0.77)	5821. -> 5496.
359.60(0.07)	1000.00(51.48)	360. -> 0.
401.39(0.61)	2.02(0.67)	2185. -> 1784.
459.10(0.75)	5.44(2.51)	
475.13(0.24)	11.37(1.67)	835. -> 360.
510.71(0.16)	77.63(9.10)	
608.27(0.29)	12.00(2.16)	6547. -> 5939.
858.11(0.17)	9.16(1.16)	2185. -> 1327.
932.67(0.11)	24.69(1.81)	
966.85(0.06)	283.35(15.03)	1327. -> 360.
986.95(0.21)	13.51(1.74)	
1014.99(0.39)	6.15(1.33)	2342. -> 1327.
1064.46(0.10)	24.54(1.75)	
1099.07(0.89)	4.58(2.90)	2882. -> 1784.
1101.16(0.43)	9.45(2.94)	
1118.58(0.44)	4.23(1.45)	5982. -> 4863.
1136.98(0.25)	6.59(1.21)	2464. -> 1327.
1175.93(0.06)	102.52(5.50)	2502. -> 1327.
1192.49(0.27)	15.23(2.11)	4863. -> 3671.
1243.24(0.12)	18.02(1.60)	2570. -> 1327.
1279.96(0.07)	61.95(3.63)	
1326.49(0.05)	342.96(17.53)	1327. -> 0.
1333.45(0.17)	18.03(1.89)	
1422.22(0.18)	30.92(4.94)	
1424.05(0.20)	27.02(4.85)	1784. -> 360.
1559.83(0.15)	16.22(1.55)	2886. -> 1327.
1610.92(0.18)	12.57(1.24)	
1768.56(0.17)	17.10(1.58)	5821. -> 4052.
1817.99(0.18)	12.22(1.28)	3144. -> 1327.
1899.08(0.15)	28.96(2.31)	
1915.85(0.37)	5.90(1.18)	
1935.25(0.20)	12.57(1.36)	3262. -> 1327.
1956.83(0.33)	9.32(1.56)	3283. -> 1327.
1960.70(0.74)	4.12(1.57)	
1982.14(0.13)	43.98(2.83)	2342. -> 360.

[1]Relative to 359.60 keV transition

Table 10. (continued)

Energy (keV)	Relative[1] Intensity	Assignment
2050.95(0.72)	2.99(1.19)	
2056.09(0.49)	4.56(1.15)	
2246.73(0.24)	14.02(1.55)	3573. -> 1327.
2254.06(0.29)	9.56(1.35)	
2341.59(0.36)	6.48(1.04)	2342. -> 0.
2351.32(0.44)	4.68(0.95)	5496. -> 3144.
2393.72(2.03)	1.78(1.61)	5280. -> 2886.
2397.83(0.24)	26.33(2.25)	5280. -> 2883.
2412.17(0.92)	2.61(1.17)	
2508.92(0.66)	3.92(1.23)	
2522.89(0.35)	8.95(1.37)	2883. -> 360.
2575.85(0.57)	3.79(1.05)	
2613.24(0.35)	7.19(1.11)	5496. -> 2882.
2656.04(0.62)	3.88(1.17)	5939. -> 3283.
2677.23(0.99)	2.28(1.17)	5939. -> 3262.
2725.77(0.24)	16.17(1.31)	4052. -> 1327.
2757.29(0.27)	12.47(1.35)	
2784.61(0.46)	4.71(1.08)	3144. -> 360.
2796.60(0.63)	3.20(1.00)	
2839.64(0.84)	2.53(1.00)	
2882.46(0.27)	13.61(1.22)	2883. -> 0.
2923.49(0.29)	17.11(1.55)	3283. -> 360.
2938.59(0.50)	4.52(0.98)	5280. -> 2342.
2988.55(0.72)	3.36(1.16)	
3079.30(1.69)	1.33(1.01)	4863. -> 1784.
3144.17(0.49)	5.64(1.16)	3144. -> 0.
3167.69(0.63)	4.01(1.16)	6741. -> 3573.
3261.58(0.44)	6.16(1.03)	3262. -> 0.
3283.35(0.31)	20.62(1.98)	3283. -> 0.
3369.18(0.95)	2.08(0.92)	5939. -> 2570.
3426.46(0.37)	8.73(1.14)	
3573.28(0.31)	23.19(1.68)	3573. -> 0.
3661.52(0.74)	2.99(0.93)	6547. -> 2886.
3786.29(0.43)	6.92(1.02)	
3797.52(0.42)	7.56(1.03)	5982. -> 2185.
3835.01(0.39)	9.26(1.07)	
3870.47(0.47)	7.13(1.16)	
3897.94(0.66)	3.40(0.88)	
3931.74(0.39)	9.41(1.10)	
4009.33(0.70)	2.60(0.65)	

Table 10. (continued)

Energy (keV)	Relative[1] Intensity	Assignment
4028.31(0.45)	5.00(0.69)	4863. -> 835.
4037.07(0.51)	3.74(0.67)	5821. -> 1784.
4085.69(0.55)	3.19(0.68)	
4145.74(1.10)	1.65(0.79)	
4178.55(0.67)	3.32(0.83)	6681. -> 2502.
4198.30(1.01)	1.77(0.69)	5982. -> 1784.
4205.49(0.71)	2.73(0.69)	6547. -> 2342.
4217.49(1.10)	1.52(0.69)	6681. -> 2463.
4238.22(0.42)	7.81(0.92)	6741. -> 2502.
4250.64(0.73)	2.60(0.70)	
4277.37(0.48)	5.08(0.74)	6741. -> 2463.
4362.91(1.62)	1.02(0.73)	6547. -> 2185.
4369.27(0.40)	10.58(1.01)	
4418.24(0.41)	8.56(0.85)	
4494.21(0.57)	3.07(0.62)	5821. -> 1327.
4537.24(1.04)	1.30(0.46)	
4549.60(0.82)	1.77(0.47)	
4564.84(0.67)	2.37(0.47)	
4578.16(0.67)	2.29(0.62)	
4609.80(0.68)	1.89(0.48)	
4647.80(0.51)	3.58(0.50)	
4670.24(1.28)	0.65(0.30)	
4681.77(0.90)	1.00(0.30)	
4694.69(0.69)	1.41(0.37)	
4730.39(1.09)	0.59(0.24)	
4738.37(1.09)	0.59(0.24)	
4812.19(0.79)	0.95(0.24)	
4862.73(1.26)	0.62(0.25)	4863. -> 0.
4891.05(0.80)	1.37(0.32)	
4896.81(0.98)	0.95(0.31)	6681. -> 1784.
4937.14(1.19)	0.47(0.19)	
4955.49(1.36)	0.39(0.18)	
4993.64(1.25)	0.43(0.18)	
5006.17(0.89)	0.78(0.19)	
5028.21(1.13)	0.46(0.19)	
5374.13(1.41)	0.40(0.13)	

Table 11. Gamma-ray coincidences in ^{142}Cs

Gate (keV)	Coincidences (keV)
20	414,572
46	572,644
72	124,157,219,414,538,571
94	124,197
124	73,94,414,547
157	73,414,538
165	414,453
191	406,414,453
197	94,414,547
203	394,406,414,453,538
211	406,1108
219	73,352
250	349,406
286	352
291	352,891
349	250
394	191,203
406	250
414	73,157,164,191,203,231,538
524	250
538	157,191,203,231,250,352,414,453,571 617,644,656
571	73,538
618	538
644	538
657	538
930	1312

Table 12. Gamma-ray coincidences in ^{142}Ba

Gate (keV)	Coincidences (keV)
100	359, 1422
359	475, 510, 858, 932, 966, 986, 1064, 1136, 1175, 1192, 1243, 1279, 1333, 1422, 1559, 1610, 1768, 1818, 1915, 1935, 1956, 1960, 2246, 2254, 2341, 2397, 2522, 2725, 2923, 2938, 3079, 3369, 3426, 3897
932	359, 1175
966	359
1064	359, 966
1175	359, 966
1279	359
1326	1015, 1137, 1243, 1818, 1935, 1956, 2246, 2725
1333	359
1422	359, 966, 986, 1326
1559	359, 966, 1326
1768	359, 1064
1899	359, 966, 1935
1935	359, 966, 1279, 1326, 1899
1982	359, 986
2246	359, 966, 1326
2254	359
2725	359, 966, 1326
2923	359

coincidence experiments are listed in Tables 11 and 12.

D. Results

The level schemes of ^{142}Cs and ^{142}Ba are shown in Figures 13 and 14. The same rules were used in constructing these level schemes as were used for those previously described for ^{101}Tc and ^{101}Ru. The transition intensities in Figures 13 and 14 are the same as in Tables 9 and 10.

Estimations of the ground state-beta branching for the level scheme of ^{142}Ba was obtained in the following manner. The intensity of the 641.17-keV gamma ray, assigned to the ^{142}La activity, was used to determine the number of ^{142}Cs decays over a given period of time. The relative amounts of Cs and La activity in the spectrum were determined by referring to the data accumulation times used, and solving for the activities from the Bateman equations. The ground-state beta branch, of 44 ± 6 %, was determined by subtracting the transition intensity feeding the ground state from the number of ^{142}Cs decays.

The procedure was modified for the ^{142}Cs levels because of the presence of a large number of low energy gamma rays that could be highly converted. If the twenty lowest energy levels (those below 1066.66 keV) are treated as a single level for beta decay purposes, beta branching for the levels at 1066.66 keV and above can be calculated without knowing the transition types. This is important since the range of

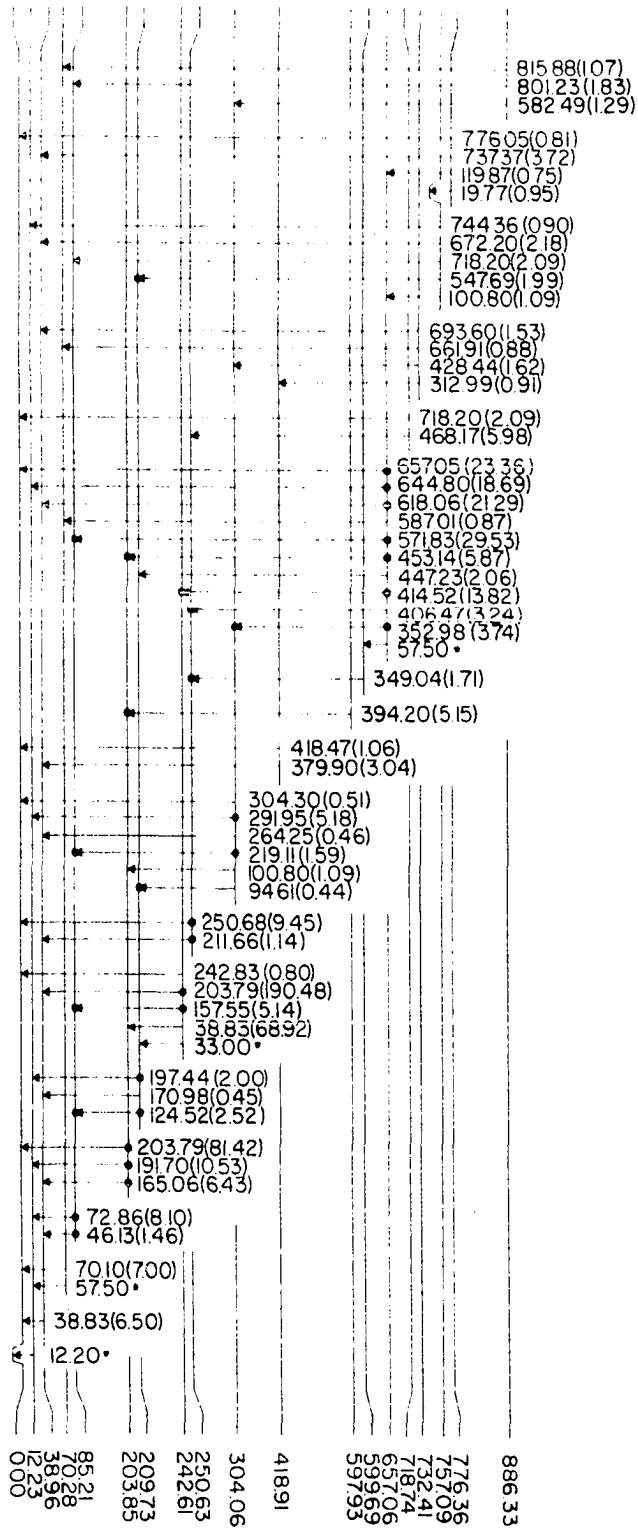

Figure 13. The ^{142}Cs level scheme

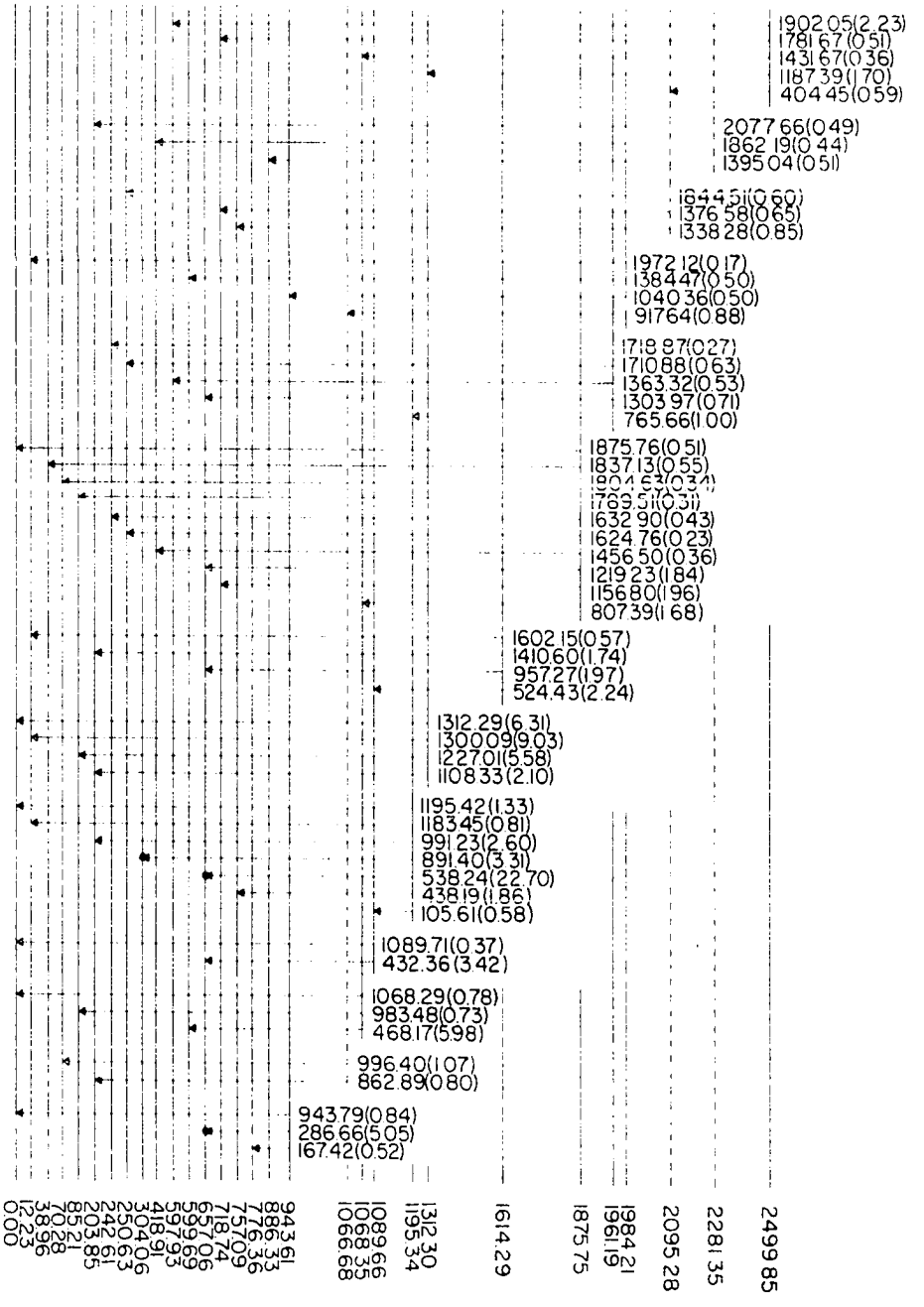

Figure 13. (continued)

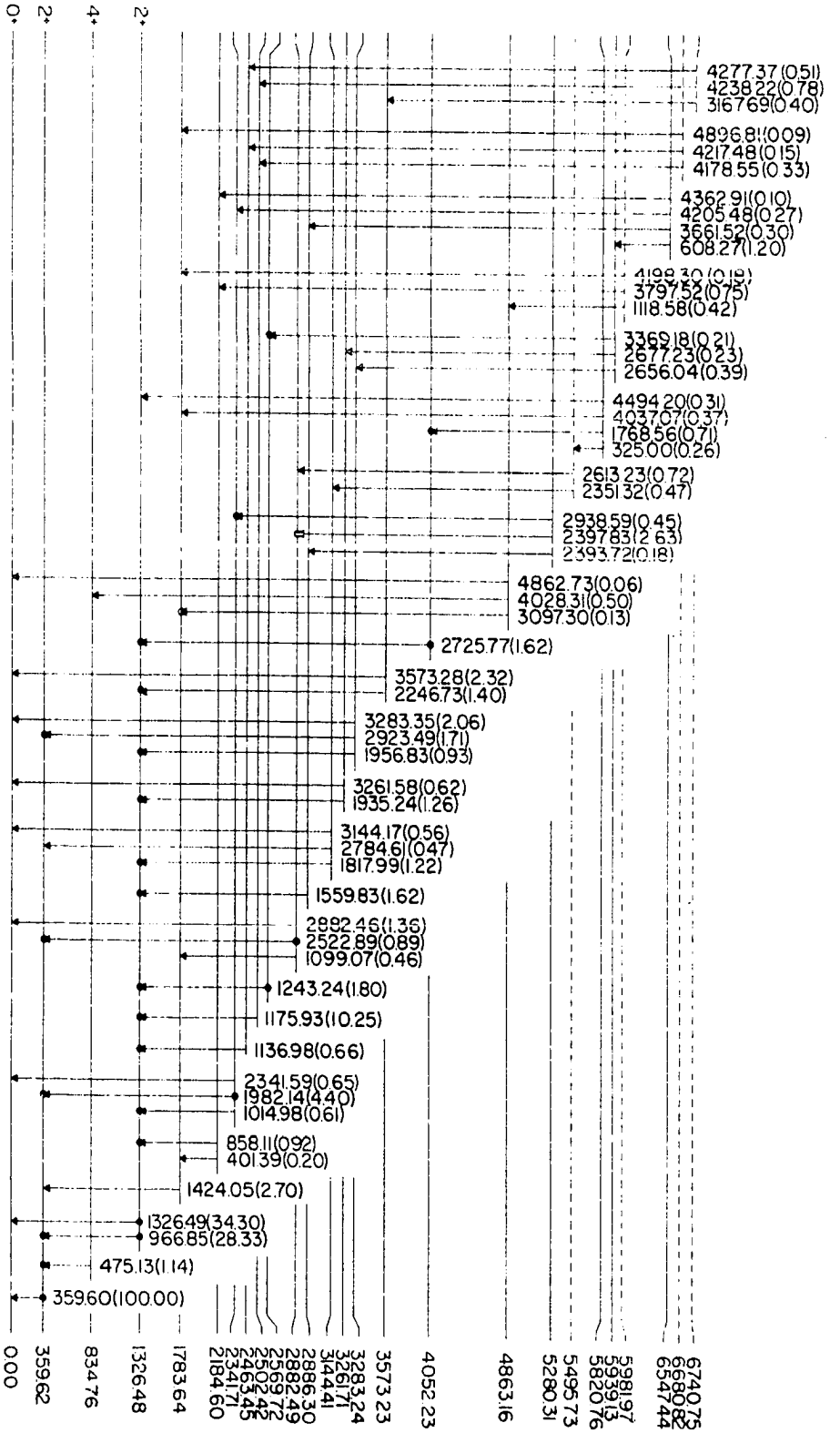

Figure 14. The $^{142}_{56}Ba_{86}$ level scheme

internal conversion coefficients (32) for E1, M1 and E2 transitions range from 0.0043, 0.0174 and 0.014 at 430.0 keV to 3.1, 14.6 and 1514.0 at 19.77 keV, respectively.

Some of the low-energy gamma rays that are indicated by coincidence experiments and decay energy sums were not seen in the singles or coincidence spectrum. It was assumed that these transitions are not seen in the gamma-ray spectrum because they are so highly converted. The minimum peak intensity that could be detected was assigned as the intensity limit of these gamma rays. This intensity was taken to be (FWHM) x 1.5 x $\sqrt{N}$, where N is the number of background counts at the peak's location and FWHM is the peak Full-Width-at-Half-Maximum. These gamma rays are noted with asterisks in Table 9.

E. Conclusions

Eleven levels were added to the decay scheme of ^{142}Xe reported by Larsen et al. (27). The new levels at 418.78, 1961.17 and 2499.87 keV have five gamma rays connecting them to other known states. The new 732.33-, 886.28-, 1089.57-, 1614.32-, 1984.24- and 2095.27-keV levels have four gamma rays associating them with other known levels. Only three gamma rays connect the 1066.66- and 2281.30-keV levels, which are dashed in the level scheme.

The log ft values for the ^{142}Cs energy levels above 943 kev, given in Table 13, indicate mostly allowed beta decay.

Table 13. Summary for beta fed levels in ^{142}Cs

Level Energy (keV)	Percent Beta Feeding	Log ft
1066	0.44(0.11)	6.33
1068	0.21(0.16)	6.66
1089	0.14(0.20)	6.81
1195	14.67(0.58)	4.75
1312	8.71(0.31)	4.92
1614	2.90(0.17)	5.23
1876	3.64(0.22)	4.98
1961	1.40(0.11)	5.35
1984	0.89(0.12)	5.53
2095	0.66(0.12)	5.59
2281	0.63(0.09)	5.48
2500	2.40(0.16)	4.75

Since the ground state of the even-even parent has a spin-parity of 0+, allowed beta decay would go to energy levels with spin-parity of 0+ or 1+. These even-parity levels probably involve an $i_{13/2}$ neutron and a $g_{7/2}$ proton. The ^{142}Cs ground state should be a $g_{7/2}$ proton coupled to an $f_{7/2}$ neutron, so most of the low-lying energy levels should have negative parity. Determination of the spins and parities of these states depends upon the low-energy gamma rays. The multipolarities for the low-energy transitions must be determined in order to solidify the ^{142}Cs level scheme, perhaps by internal conversion electron measurements. Until this is done, the spin-parity assignments of the low-energy levels cannot be made.

Twenty-one new levels have been added to the ^{142}Ba level scheme of Larsen et al. (27). The level at 2882.49 keV is supported by five gamma rays, two of which are listed as coincidences. The 3283.24-keV state is connected to four other energy levels and two of these gamma rays are listed as coincidences. One coincident, and three additional gamma rays connect the states at 2184.60, 3144.41, 5820.31 and 5939.13 keV to other known levels. The new levels at 4863.16 and 6547.44 keV are supported by four gamma rays leading to other known states. The 5280.31-keV level is connected to three other levels, two of these levels by coincident gamma rays. Three gamma rays, one of which is

listed as coincident, connect the 2463.45-,2502.42-, on 2463.45-, 2502.42-, 2886.30-, 3261.71- and the 3573.23-keV levels to other known states. Three non-coincident gamma rays connect the levels at 5495.73, 5981.97, 6680.82 and 6740.75 keV to other known states and they are dashed to indicate their lack of firmness. The levels at 2569.72 and 4052.23 keV are associated with two gamma rays, both of which are listed as coincidences. The new level at 834.76 keV is supported by two connecting gamma rays, one of which is listed in the coincidence table.

Not enough supportive evidence was present in this work to confirm the existence of five levels reported in the partial level scheme given by Larsen et al. (27). The levels at 1423, 1639 and 2128 keV are supported only by a single coincident gamma ray. Two gamma rays, one of these coincident, connect the 1535-keV level to two other states. However, the 208.8 keV gamma ray was not detected in this work. The level at 2757 keV is connected to three other levels by gamma rays not seen in the coincidence experiments. Two of the three gamma rays were seen in this work but the CI is too low (<4) for a level to exist.

The log ft values of the ^{142}Cs beta decay are listed in Table 14. With the ground state of ^{142}Cs probably being negative parity, the "allowed" beta decay indicated by the ground-state branch log ft would give negative parity to the

Table 14. Summary for beta fed levels in ^{142}Ba

Level Energy (keV)	Percent Beta Feeding	Log ft
	44.00(6.00)	5.59
359	24.38(2.14)	5.75
834	0.25(0.07)	7.59
1326	15.52(0.93)	5.63
1783	0.49(0.23)	6.98
2184	0.10(0.07)	7.50
2342	1.91(0.13)	6.17
2502	3.50(0.22)	5.84
2569	0.62(0.07)	6.56
2886	0.44(0.09)	6.57
3144	0.69(0.09)	6.25
3262	0.64(0.08)	6.22
3283	1.67(0.12)	5.79
3573	1.28(0.09)	5.75
4052	<0.04	>6.95
4869	0.10(0.07)	5.96
5280	1.26(0.11)	4.49
5496	0.35(0.07)	4.81
5821	1.03(0.07)	3.91
5982	0.52(0.01)	3.94
6547	0.73(0.09)	2.35
6681	0.22(0.04)	2.19
6741	0.65(0.06)	1.27

even-even ground state of ^{142}Ba. This, of course, is unreasonable and the apparently low log ft values are a strong indication that serious problems exist with this level scheme.

The spin and parity assignments of the low-lying ^{142}Ba energy levels are made on the basis of nuclear systematics. The 4+ state at 834 keV that Larsen et al. alluded to has been firmly established. This state is predicted by observing neutron pairs being added to ^{138}Ba. Another interesting structure note in this region is illustrated in Figure 15. It appears that low-energy structures of Ba nuclei 2n-neutron pairs below N=82 are similar to those of Ba nuclei n-neutron pairs above N=82 (33). Further attempts to fit this nucleus to a specific model must be delayed until the level scheme is on firm footing. The bootstraping procedure used to determine the energies of gamma rays above 3500 keV appears to be adequate and it is hoped that the serious problems with this level scheme can be resolved by a closer analysis of the coincidence data. The possibility exists that the relatively important 966-, 1064-, 1175-, and 1326-keV gamma rays are doublets and detailed interpretation of the coincidence data should indicate their placement.

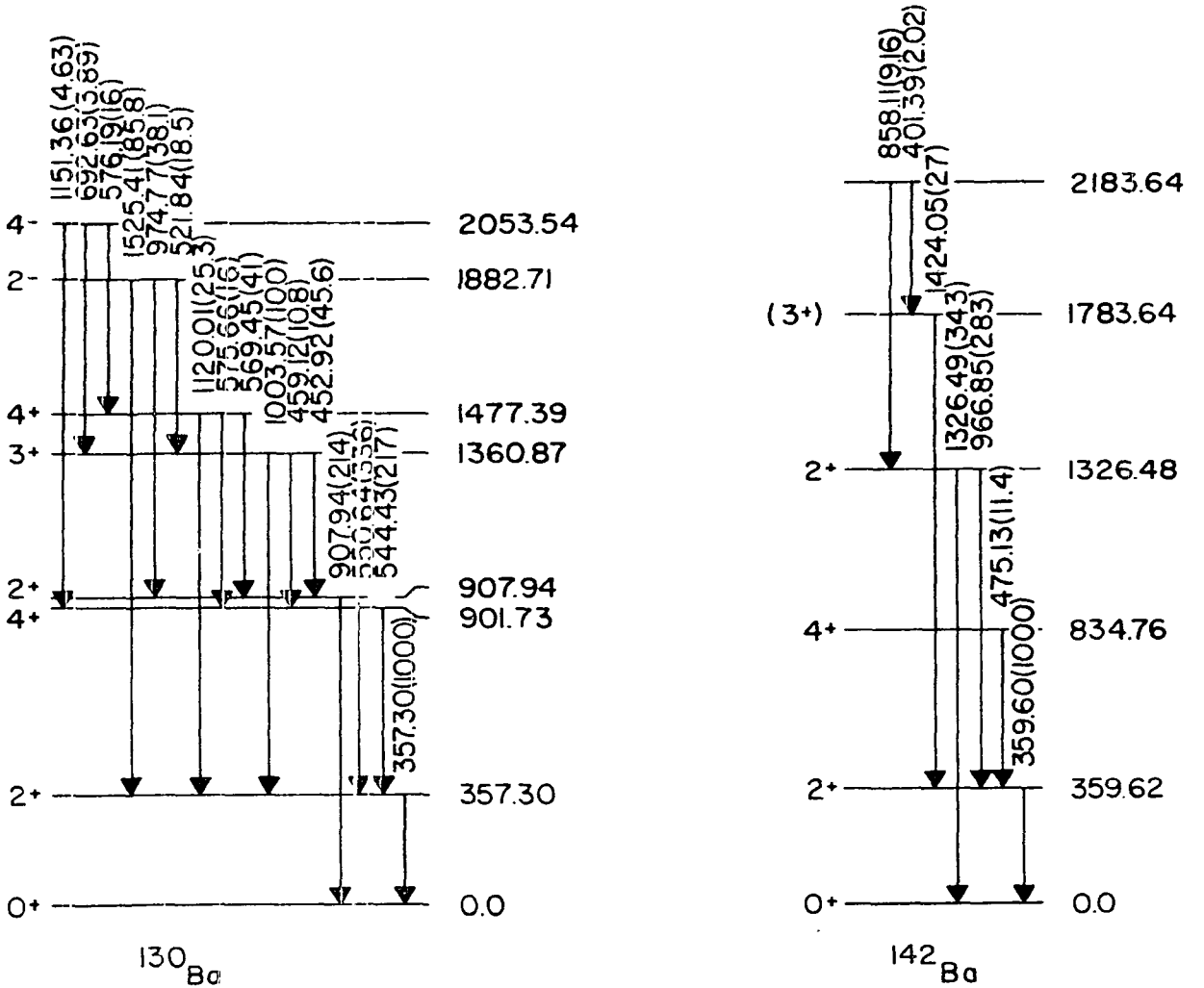

Figure 15. The comparison of ^{130}Ba and ^{142}Ba levels

IV. APPENDIX A: COMPUTER PROGRAMS

A. SKEWGAUS

Due to the non-Gaussian shape of Ge(Li) photopeaks, the computer program SKEWGAUS was used to determine the areas and exact location of these gamma-ray peaks. For fitting purposes, each peak is divided into three regions by SKEWGAUS. A linear or quadratic background is constructed, and then allowed to vary with the other peak parameters to give a best fit to the data.

The functions used are:

Region	Function
1	$N\{e^{-X_0(2X-X_0)}[1-A+B(X+X_0)^4]+A\}$
2	$N\{e^{-X^2}(1-A)+A\}$
3	$N\{e^{-X^2}(1-CX^5)\}$

where $X = \frac{E_p - E}{\sqrt{2}\,S}$

E_p is the centroid energy and S is the Gaussian standard deviation. E_0 is the "crossover energy", and is determined from X_0.

Region 1 contains an exponential function, a backscatter tail(A), and a skewness term(B). Region 2 contains a pure Gaussian plus a backscatter tail(A), and includes both $E=E_0$ and $E=E_p$. Region 3 contains a pure Gaussian plus a skewness term(C). The backscatter tail(A) is generally used only on data taken with a Si(Li) detector. The low-skewness parameter(B) is usually used for intense, low-energy peaks. The skewness parameter(C) on the high-energy side of the peak is needed usually only when the counting electronics are improperly adjusted or the count rate is too high.

In practice the parameters A, B, and C are generally set to zero for Ge(Li) spectra. The "Full-Width-at-Half-Maximum" is easily measured experimentally and is defined by

$$FWHM = \sqrt{8(\ln 2)}\,S \ .$$

The "crossover energy", E_0, is given by $T = (E_p - E_0)$. The parameters T and FWHM are fit to a linear energy dependence using several well-defined photopeaks, and then can be held to this dependence in the data fits. The functions are fit to the data by using Gauss's iteration method of non-linear least squares. The errors in the parameters (34) are the square roots of the diagonal terms in the error matrix of the fit.

B. DRUDGE

Cards which can be punched as an option by SKEWGAUS contain the locations of the peak centroids, the peak areas, the peak heights and the errors in the centroids and peak heights. DRUDGE calculates the energies, intensities, and the associated errors of the peak energies and intensities.

Three separate spectra are needed to calculate the gamma ray energies. The first is a spectrum of well known standards, used to determine the integral non-linearity of the counting system. The second spectrum contains the standards plus the unknown source. From this spectrum, the energies of intense, unknown peaks can be determined. The last spectrum is of the unknown sample only. The energies of the peaks determined in the second spectrum are used to determine the energies of the remaining gamma-ray peaks.

The intensities of the unknown gamma rays are determined by making the proper corrections to the peak areas determined by SKEWGAUS. Detector relative efficiency is determined by using well-known standards. DRUDGE also aids in identifying single-escape peaks, double-escape peaks and Compton edges. The possible escape peaks are determined by comparing the ratios of the photopeak intensity to the single- or double-escape peak intensity. The possible Compton edges are determined by comparing the Compton-edge energies to the photopeak energies.

C. LVLSURCH

LVLSURCH is a computer program that will extend a preliminary decay scheme, in which some levels are already known, to a more complete one. The input to the program consists of these known levels, the known gamma rays and coincidence information. The program checks the known gamma rays with the known levels to see if any new levels can be constructed. Restrictions placed on this operation are: 1) the difference between two energy levels must be within a certain tolerance of the gamma-ray energy. 2) A predetermined number of gamma rays must enter or leave a level for the program to accept it as a new level. 3) The gamma rays used to determine the new levels must not violate the coincidence information. After the new levels are determined, they are merged with the old levels, then the program repeats the search using this mixed set as the new starting levels.

D. Auxiliary Programs

TICC is a FORTRAN program that calculates the total internal conversion coefficient of a transition from the K, L and M conversion coefficients. The coefficients are determined by a log-log interpolation from the Hager and Seltzer tables (32). Either pure or mixed (50%E2 + 50%M1) transition types can be used in the calculations.

LEAF is a secretary program that compiles the gamma rays placed in a level scheme, and calculates the best level energies and the percent beta feedings to these levels. The gamma-ray intensities are also corrected for internal conversion processes, if the output of TICC is furnished with the gamma-ray list.

The log ft values for each level were calculated using the program LOGFT. This program uses the percent beta branching to actually calculate the Fermi function with either a statistical or unique first-forbidden shape factor. The calculation also includes compensation for atomic screening effects.

V. APPENDIX B: EXPERIMENTAL NOTES

A. Detectors

Table 15. Detectors used in experiments

Detector geometry	Active volume ($cm.^3$)	Resolution @ energy (keV)	Efficiency	Peak/Compton for 1332-keV gamma ray
true coaxial	57.3	2.3 @ 1332.48	11.8%	34/1
true coaxial	58.2	2.3 @ 1332.48	9.%	28/1
planar	1.0	.650 @ 122.	N/G	N/G
trapezoidal	26.3	2.84 @ 1332.48	2.6%	14/1
trapezoidal	29.7	3.84 @ 1332.48	3.5%	12/1
trapezoidal	39.0	3.1 @ 1332.48	4.3%	16/1

B. Gamma Ray Calibration Sources

Table 16. Gamma-ray calibration standards

Nuclide	Gamma ray energies (keV)
^{56}Co [a]	846.71,1037.82,1175.07,1238.25, 1360.17,1771.30,1810.67,1963.68, 2015.14,2034.71,2113.06,2212.86, 2598.40,3009.52,3201.89,3253.35, 3272.92,3451.07,3547.64
^{57}Co [a]	14.411,122.060,136.471
^{186}Ta [a,b]	31.376,42.715,67.750,84.680,100.105, 113.673,116.418,152.433,156.387, 179.393,198.351,222.110,229.322, 264.072,1121.28,1189.03,1221.38, 1230.99,1257.39,1273.71,1289.13
^{226}Ra [b]	186.14,241.96,295.20,351.92,609.278, 665.40,742.48,768.35,785.80,806.16, 934.06,1120.28,1155.17,1238.13, 1280.98,1377.64,1401.44,1407.98, 1509.22,1661.24,1729.55,1764.49, 1838.33,1847.44,2118.52,2204.14, 2447.63

a. R. C. Greenwood et al. (35-37)
b. R. Gunnink et al. (38)

C. Singles Collection

The circuitry (Figure 16) for singles collection normally consisted of a large detector, an Ortec Model 120-28 preamplifier, a Tennelec Model TC203BLR linear amplifier, a 13-bit ADC and a 16,384-channel modified TMC analyzer. A four sec time constant, base-line restoration, and DC coupling between the main amplifier and the ADC usually produced the best system resolution and peak shape.

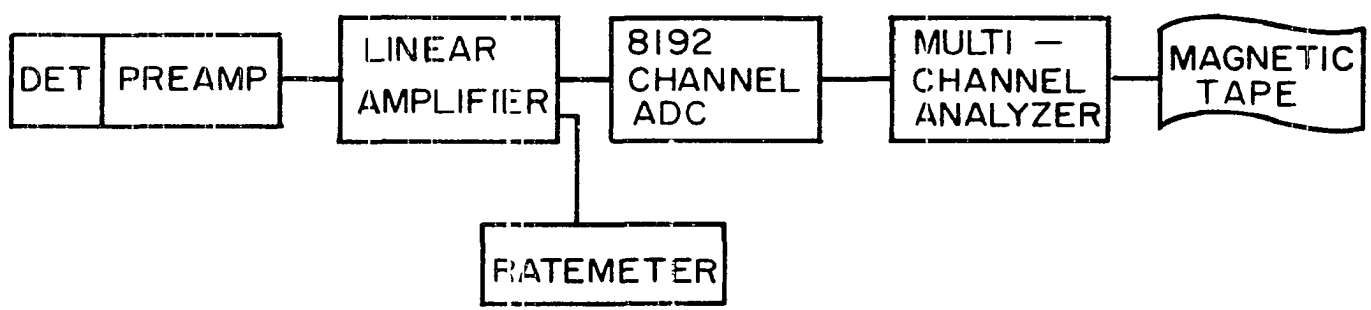

Figure 16. Block diagram of circuitry for singles collection

D. Two-Parameter System

The TRISTAN two-parameter counting system allows the signals from two sources to be recorded pair by pair to give the capability of replaying the experiment and containing all data necessary to build a 4096 X 4096 "histogram surface". If an event from source A is "related" to an event from source B, the addresses of the events in A and B are stored as a pair of numbers in a buffer memory. The most common way to use the system is to have the energy dependent outputs of the Ge(Li) detectors as the sources of signals A and B. For example, if a gamma ray from detector A occurred within a coincidence time window of a gamma ray from detector B, the addresses from the ADC's A and B, would be stored in the buffer memory as successive word pairs. When this memory fills up, its contents are placed on magnetic tape. At the end of the experiment, it is possible to recall from magnetic tape all events from detector A that were recorded in coincidence with an arbitrary channel interval for detector B. A block diagram of the electronics used with the two-parameter system is shown in Figure 17.

BUFFTAPE is an Assembler Language program that reads magnetic tapes from the two-parameter system and sorts the information into bands. Each band contains a spectrum that was in coincidence with a gating energy window. The spectrum in coincidence with a particular photopeak was

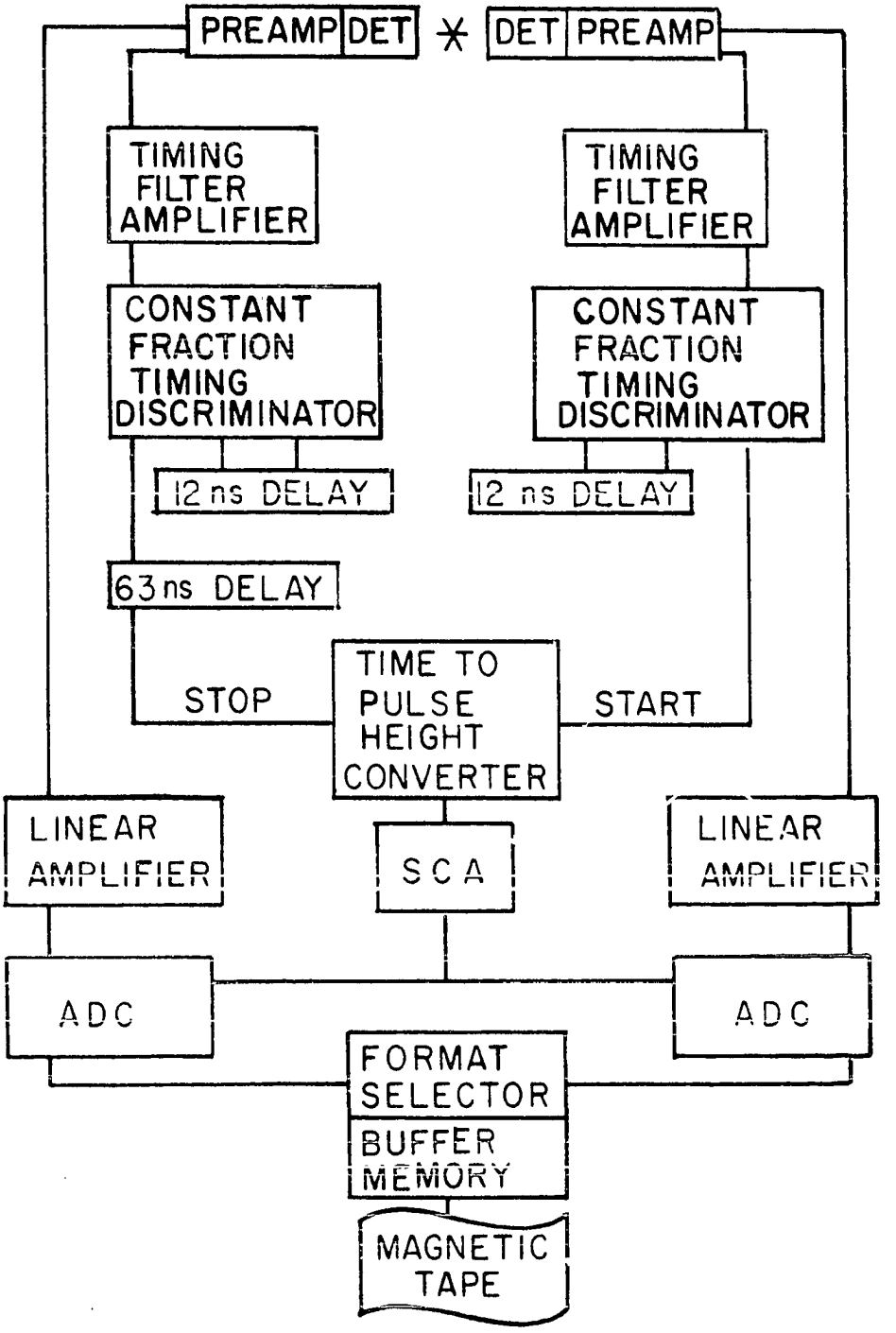

Figure 17. Block diagram for circuitry in coincidence experiments

obtained by including the most prominent part of the peak in the gating window. The spectrum in coincidence with the background of the photopeak was obtained by dividing the gating window into two parts and setting them at a higher and lower energy than the photopeak. Care was taken to insure that the background gates were free from other photopeaks and that the number of channels in the background gate was equal to the number of channels in the peak gate.

VI. APPENDIX C: THEORETICAL NOTES

A. Neutron Single-Particle States (50<N<62)

Figure 18 shows the neutron single-particle states (27) for the region near 58 neutrons. The $g_{7/2}$ and $s_{1/2}$ neutron states are lowered in energy as the total number of nucleons is increased. However, the $g_{7/2}$ level falls faster than the $s_{1/2}$ and at N=58, the $g_{7/2}$ should be filled. A configuration other than $(g_{7/2})^8$ would require the breaking of a pair of these neutrons. Since the pairing energy varies like j+1/2, it seems reasonable to assume that the configuration of the outer eight neutrons of ^{101}Tc is $(g_{7/2})^8$.

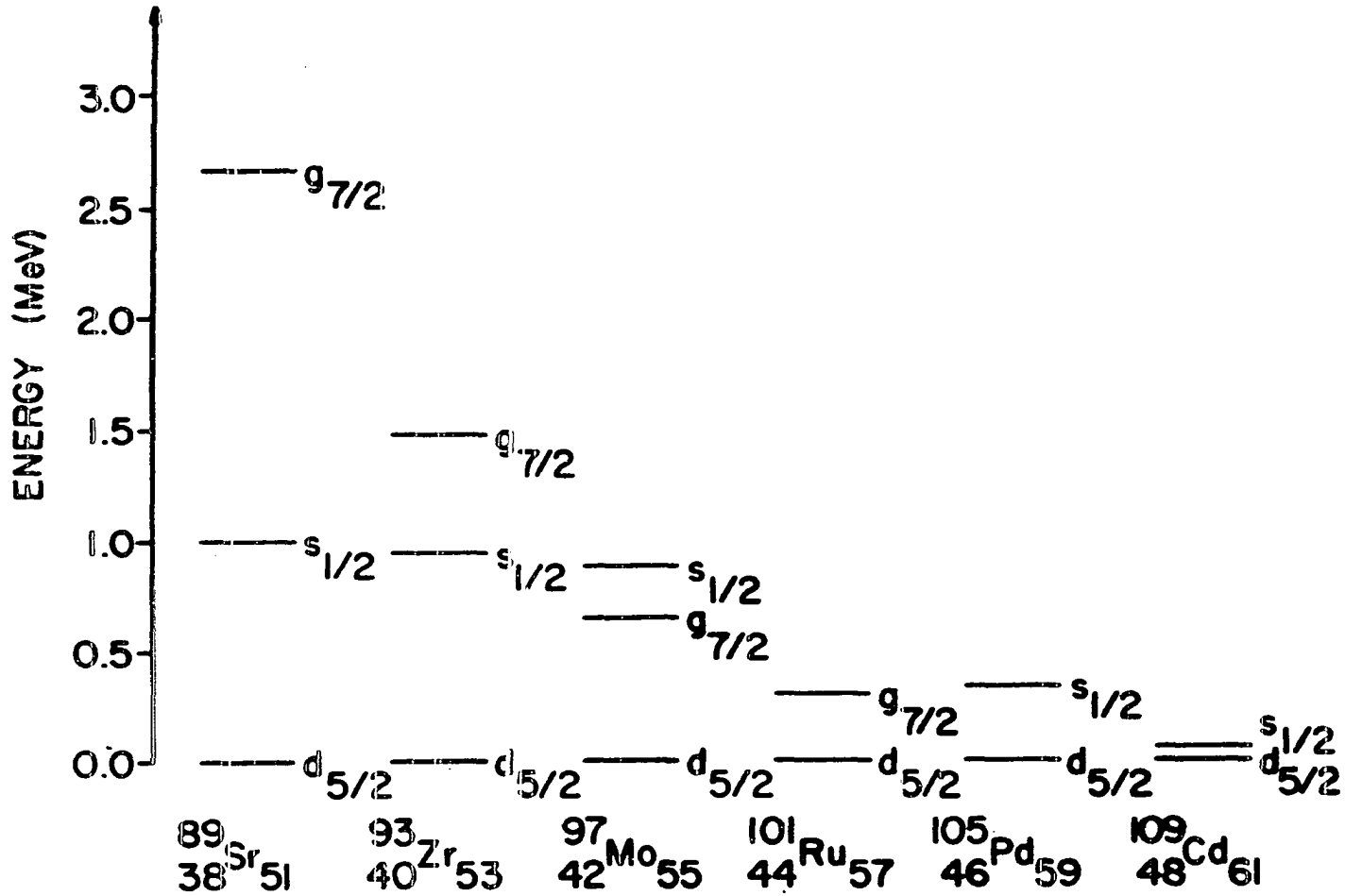

Figure 18. Neutron single-particle states

B. Special Many-Particle Wave Functions

Using group theoretical techniques, a totally antisymmetric n-body wave function can be constructed from 2 antisymmetric p-body and q-body wave functions, where p+q=n (8). This wave function is defined by equations (c.1) and (c.2).

$$|\alpha J> = N\{\underline{e} + \sum_{i=1}^{p}\sum_{j=p+1}^{n} \underline{P}(ij)\,[\sum_{\ell>i}\sum_{m>j}^{p,n} \underline{P}(\ell m) - 1\,]\} \times |1\ldots p;p+1\ldots n> \qquad (c.1)$$

$$|1\ldots p;p+1\ldots n> = [\,|1\ldots p,J_1> \otimes |p+1\ldots n,J_2>\,]^{J} \qquad (c.2)$$

The identity operator is given by $\underline{e}$, $\underline{P}(i,j)$ is the operator that permutes particles i and j and N is the normalizing constant. Equation (c.3) gives the result for the five-body case.

$$\begin{aligned}|\alpha J> = \frac{1}{\sqrt{10}}\{\ & |12,345> - |32,145> - |42,315> - \\ & |52,341> - |13,245> - |14,325> - |15,342> + \\ & |34,125> + |35,142> + |45,312>\ \} \end{aligned} \qquad (c.3)$$

VII. LITERATURE CITED

1. N. Auerbach and I Talmi, "Energy Levels, Configuration Mixing and Proton Neutron Interaction in the Zr Region," Nucl. Phys. A64, 458 (1965).

2. J. Vervier, "Effective Nucleon-Nucleon Interactions in the Y, Zr, Nb, Mo, and Te Isotopes," Nucl. Phys. A75, 17 (1966).

3. M. G. Mayer, "Nuclear configurations in the spin-orbit coupling model I. Empirical evidence," Phys. Rev. 78, 16 (1950).

4. R. R. Roy and B. P. Nigam, Nuclear Physics, (John Wiley and Sons, Inc., New York, 1967), p. 231.

5. A. de-Shalit and I. Talmi, Nuclear Shell Theory, (Academic Press, Inc., New York, 1963), p. 104.

6. M. Rotenberg et. al., 3j, 6j and 9j Symbols, (Mass. Inst. Tech. Press, Cambridge, 1959).

7. M. E. Rose, "Elementary Theory of Angular Momentum," (John Wiley and Sons, Inc., New York, 1957).

8. S. A. Williams, Ames Laboratory, Private Communication (1973).

9. B. Siwamogsatham and H. T. Easterday, "Note on the ^{101}Tc-^{101}Ru decay," Nucl. Phys. A162, 42 (1971).

10. N. K. Aras, P. Fettweis, G. Chilosi, and G. D. O'Kelley, "Levels in ^{101}Ru populated by the decay of ^{101}Tc," Nucl. Phys. A169, 209 (1971).

11. W. B. Cook and M. W. Johns, "Decay of ^{101}Mo and ^{101}Tc," Can. J. Phys. 50, 1957 (1972).

12. A. V. Aldushchenkov, et al., "Three-Particle and Anomalous Excited States of the Nucleus ^{101}Tc," Izv. Akad. Nauk SSSR, Ser. Fiz. 37. 965 (1973).

13. W. B. Cook, M. W. Johns, J. S. Geiger, and R. L. Graham, "Low-Lying Positive-Parity States in ^{101}Tc," Can. J. Phys. 50, 1511 (1972).

14. L. K. Peker and V. M. Sigalov, "Anomalous Isomerism of Odd Tc Isotopes with A ≥ 101," Izv. Akad. Nauk. SSSR Ser. Fiz. 34, 1782 (1970).

15. J. Uyttenhove, J. Demuynck, M. Dorikens, and L. Dorikens-Vanpraet, "Experimental Study of the Isomeric States of ^{101}Ru, ^{103}Ru and ^{101}C," Z. Physik. 238, 90 (1970).

16. P. D. Bond, J. D. McGervey, and S. Jha, "Measurements of Some Nuclear Lifetimes in the Nanosecond Region," Nucl. Phys. A163, 571 (1971).

17. C. M. Lederer, J. M. Hollander, and I. Perlman, Table of Isotopes, sixth edition, (John Wiley & Sons, Inc., New York, 1968)

18. K. Ueno and C. T. Chang, U. S. Atomic Energy Commission Report No. JAERI-1036, 1962 (unpublished).

19. N. K. Aras, P. Fettweis, G. Chilosi, and G. D. O'Kelley, "Levels in ^{101}Ru populated by the decay of ^{101}Tc," Nucl. Phys. A169, 218 (1971).

20. G. D. O'Kelley, Q. V. Larson, and G. E. Boyd, "Decay chain ^{101}Mo-^{101}Tc," Bull. Am. Phys. Soc. 2, 24 (1957).

21. S. Raman and N. B. Gove, "Rules for Spin and Parity Assignments," Phys. Rev. 7, 1955 (1973).

22. O. C. Kistner and A. Schwarzschild, "Coulomb Excitation of ^{99}Ru and ^{101}Ru," Phys. Rev. 154, 1182 (1967).

23. J. Sieniawski, H. Pettersson and B. Nyman, "Decay Studies of ^{101}Rh," Z. Phys. 245, 81 (1971).

24. C. M. Lederer, J. M. Jaklevic and J. M. Hollander, "Levels of ^{97}Ru, ^{99}Ru and ^{101}Ru populated in (,xn) Reactions," U. S. Atomic Energy Commission Report No. UCRL-19530, 1969 (unpublished).

25. G. H. Fuller and V. W. Cohen, "Nuclear Spins and Moments," Nuclear Data Tables A5, 433 (1969).

26. D. J. Horen and W. B. Ewbank, Nuclear Level Schemes A=45 Through A=257 from Nuclear Data Sheets, edited by Nuclear Data Group, Oak Ridge National Laboratory, (Academic Press, New York, 1973).

27. J. T. Larsen, W. L. Talbert, Jr. and J. R. McConnell, "Gamma-Ray Studies of the Decays of ^{142}Xe, ^{142}Cs, ^{142}Ba and ^{142}La," Phys. Rev. C3, 1372 (1971).

28. J. P. Adams, G. H. Carlson, M. A. Lee, W. L. Talbert, Jr., F. K. Wohn, J. R. Clifford and J. R. McConnell, "Decay energies of gaseous fission products and their daughters for A=138 to 142," Phys. Rev. C8, 767 (1973).

29. G. C. Carlson, W. C. Schick, Jr., W. L. Talbert, Jr. and F. K. Wohn, "Half-Lives of some Short-Lived Mass-separated Gaseous Fission Products and their Daughters," Nucl. Phys. A125, 267 (1969).

30. W. L. Talbert and J. R. McConnell, "Preparation for On-Line Studies of Short-Lived Nuclei Produced by a Reactor," Ark. Fys. 36, 99 (1967).

31. J. H. Norman, W. L. Talbert, Jr. and D. M. Roberts, United States Atomic Energy Commission Report IS-1892, Iowa State University, 1968 (unpublished).

32. R. S. Hager and E. C. Seltzer, "Internal Conversion Tables, Part I: K-, L-, M-Shell Conversion Coefficients for Z = 30 to Z = 103," Nuclear Data 4, 41 (1968).

33. R. A. Meyer, Lawrence Livermore Laboratory, Private Communication (1974).

34. E. A. Henry, "Gamma-ray decay schemes for ^{89}Kr and ^{89}Rb," U. S. Atomic Energy Commission Report No. IS-T-520, Iowa State University, 1972 (Unpublished).

35. R. C. Greenwood, R. G. Helmer and R. J. Gehrke, "Precise Comparison and Measurement of Gamma-ray Energies," Nucl. Instr. Methods 77, 141 (1970).

36. R. G. Helmer, R. C. Greenwood and R. J. Gehrke, "Precise Comparison and Measurement of Gamma-ray Energies," Nucl. Instr. Methods 96, 173 (1971).

37. R. C. Greenwood, National Reactor Testing Station, Private Communication (1972).

38. R. Gunnink, R. A. Meyer, J. B. Niday and R. P. Anderson, "Gamma-Ray Energy and Intensity Measurements Using Ge(Li) Detectors," U. S. Atomic Energy Commission Report No. UCID-15439, 1969 (unpublished).

VIII. ACKNOWLEDGEMENTS

The author would like to thank the following people for their assistance during this study:

Dr. A. F. Voigt for financial support during my graduate career and for the understanding he exhibited in allowing me to study in fields of my choice.

Dr. W. L. Talbert, Jr. for his assistance and guidance in directing parts of my research and in the writing of this thesis.

Dr. B. S. Cooper for directing the theoretical portion of this thesis and, most of all, for providing stimulating and thought provoking ideas about nuclear structure and life.

John R. McConnell for his instruction in the operation of TRISTAN and for his many hours spent maintaining and developing the system.

My colleagues, Dr. J. A. Morman, Messrs. C. J. Bischof and M. D. Glascock for our many interesting discussions, sometimes even concerning physics.

Ms. Linda K. Canon for the countless hours of transferring thousands of numbers to FORTRAN coding forms.

To all the members of Nuclear Physics Group VII and Radiochemistry Group I who assisted in the data collection.

Finally, thanks to Rae, Kim and Pat for their 4-1/2

years of patience and understanding while sometimes living without a husband and father.